Physica B 179 (1992) 133–156
North-Holland

PHYSICA B

Field applied molecular dynamics (FMD) computer simulation of circular dichroism and optical rotatory dispersion

The discovery by FMD of bi-axial Rosenfeld birefringence

M.W. Evans[1], S. Woźniak[2] and G. Wagnière

Institute of Physical Chemistry, University of Zurich, Winterthurerstrasse 190, CH 8057 Zurich, Switzerland

Received 13 August 1991
Final revised 26 November 1991

Field applied molecular dynamics (FMD) computer simulation is used to investigate circular dichroism (CD) and optical rotatory dispersion (ORD) in the picosecond time window (far infrared frequency interval) using second order rise transients (RSs) and a range of time correlation function (CFs) in the presence of right and left circularly polarised (cp) lasers propagating in (a) chiral (*S*)-CHBrClF; and (b) archiral liquid water. In case (a) simulated RSs and CFs are computed using the torque mediated by the Rosenfeld tensor, and are found to be different for right and left cp lasers, and the FMD results are expressed in terms of a set of novel pseudoscalar, difference CFs. Detailed agreement is found between the RTs and analytical Langevin–Kielich functions, and the first far infrared ORD spectrum isolated in terms of a novel rotational velocity difference CF for different applied laser intensities. In case (b), pseudoscalar difference functions between right and left cp lasers are not observed, indicating that there is no CD or ORD in water, but a novel anisotropy develops due to surviving off-diagonal elements of the Rosenfeld tensor in water.

1. Introduction

Fresnel [1] in 1824 realised that the rotation of the plane of polarisation of electromagnetic radiation by an optically active material is an expression of the fact that left and right circularly polarised light interacts differently with such a medium. Interesting descriptions of the early attempts to understand this in terms of molecules have been given by Mason [2] and by Barron [3]. Among the earliest successful applications of quantum mechanics to the problem was that of Rosenfeld [4], who described optical activity through the second rank, *T* positive, *P* negative, imaginary part of the electric dipole/magnetic dipole molecular property tensor ${}^e\alpha_{ij}^m$. In semi-classical theory [3] ${}^e\alpha_{ij}^m$ is in general complex and frequency dependent and can be written in terms of beta and gamma components [5, 6]; (see eqs. (10) and (11)):

$$ {}^e\alpha_{ij}^m = {}^e\hat{\beta}_{ij}^m + \mathrm{i}\,{}^e\hat{\gamma}_{ij}^m \,. \tag{1} $$

Near optical resonance in semi-classical theory, the components ${}^e\hat{\beta}_{ij}^m$ and ${}^e\hat{\gamma}_{ij}^m$ each become complex [3, 5, 6]:

$$ {}^e\hat{\beta}_{ij}^m = {}^e\beta_{ij}^m + \mathrm{i}\,{}^e\beta_{ij}^{m\prime} \,, \tag{2} $$

$$ {}^e\hat{\gamma}_{ij}^m = {}^e\gamma_{ij}^m + \mathrm{i}\,{}^e\gamma_{ij}^{m\prime} \,. \tag{3} $$

The component ${}^e\gamma_{ij}^m$ is responsible for optical rotatory dispersion (ORD), and ${}^e\gamma_{ij}^{m\prime}$ for circular dichroism (CD) across the complete range of electromagnetic frequencies. The evolution of experimental and theoretical understanding of CD and ORD has occurred from ultraviolet and visible frequencies (electronic mechanisms [7]) to

Correspondence to: M.W. Evans, 433 Theory Center, Cornell University, Ithaca, NY 14853, USA.
[1] Permanent address: 433 Theory Center, Cornell University, Ithaca, NY 14853, USA.
[2] Permanent address: Nonlinear Optics Division, Institute of Physics, A. Mickiewicz University, Grunwaldzka 6, 60-780 Poznań, Poland.

infrared frequencies [8–10], where vibrational effects become important. The experimental technique has reached frequencies on the edge of the far infrared range [11–13], corresponding to about $100\,cm^{-1}$. It might soon be possible to investigate spectrally the fundamental rotation/transition molecular dynamics of CD and ORD.

This paper anticipates this development with the first computer simulation of far infrared ORD and CD using the method of field applied molecular dynamics (FMD). This was first developed [14] to investigate the molecular dynamics of ensembles under the influence of a static homogeneous electric field, and successfully reproduced thermodynamic averages that develop in response to the applied field, the Langevin and Kielich functions. This early FMD technique resulted in the discovery of fundamental ensemble properties such as fall transient acceleration [15], field decoupling [16], and a set of novel statistical cross correlations which appear in the laboratory frame (X, Y, Z) in response to the field [17, 18]. FMD was later extended [19–23] to simulate the interaction of the electric field of a laser with the permanent electric dipole moment of both achiral [24] and chiral [25] ensembles, to circular flow [26], shear flow [27], and to electrorheology [28], resulting in the isolation of novel asymmetric cross correlation functions (CCFs) fundamental to the understanding of non-Newtonian rheology in atomic ensembles.

Recently, the FMD method has been developed for general use in non-linear optics. Each non-linear optical effect [29–35] has its characteristic torque, generated between laser and molecule.

In each relevant case, the FMD method applied to well known non-linear optical effects [36–39] (such as the optical Kerr effect) has successfully reproduced the appropriate Kielich function by coding the torque for each molecule into the forces loop of a standard molecular dynamics algorithm (of any relevant type), and generating rise transients to the point of saturation. The simulated Kielich function is then a plot of saturation level of the rise transient versus the energy of interaction per molecule of laser and ensemble. Not only does the technique accurately reproduce available analytical Kielich functions, but it also describes in great detail the nature of the molecular dynamics in the statistically stationary state in the presence of the laser, something which is inaccessible analytically. Thus far, the following non-linear optical phenomena have been FMD simulated: (1) dynamic electric polarisation [40, 41] due to the non-linear conjugate product of a circularly polarised laser; (2) the frequency doubled (or dynamic) optical Stark effect [42]; (3) the optical Kerr effect [43]; (4) the inverse Faraday effect [44]: (5) inverse magnetochiral birefringence [44]; (6) optical Zeeman effects and optical NMR and ESR [45–47]. In cases (1), (2), (4), and (5), FMD revealed fundamentally novel types of second order orientational rise transients (RTs) for which there are no Kielich functions, because the time average of the interaction energy vanishes. In cases (3) and (6), Kielich functions are defined analytically, and were accurately reproduced in the FMD simulation. Additionally, FMD revealed in great detail the nature of the molecular dynamical response of an ensemble to an intense laser, both in the RT condition and in the laser applied steady state following transient saturation. The FMD method was also able to reproduce the magnetisation [44, 48–50] of the inverse Faraday effect through the $t \rightarrow \infty$ value of the simulated molecular angular momentum autocorrelation function (ACF).

The FMD simulation of ORD and CD is one of the severest tests of the technique because it has to distinguish between the fundamentally significant but subtly different effects of right and left circularly polarised radiation on an ensemble of structurally chiral molecules, modelled [51–55] with the appropriate site–site potential. This is effectively the problem posed by Fresnel [1] expressed in terms of fundamental molecular rotation and translation on a picosecond time scale (far infrared frequency range). In this paper, the problem is approached via the field molecule interaction energy

$$E_n = -\tfrac{1}{2}\boldsymbol{\mu}^{(\mathrm{ind})} \cdot \boldsymbol{E}^* - \tfrac{1}{2}\boldsymbol{m}^{(\mathrm{ind})} \cdot \boldsymbol{B}^* + \mathrm{c.c.}\,, \qquad (4)$$

where $\boldsymbol{\mu}^{(\mathrm{ind})}$ and $\boldsymbol{m}^{(\mathrm{ind})}$ are the electric and mag-

netic dipole moments induced in a molecule, respectively, by the magnetic field $\boldsymbol{B}$ and electric field $\boldsymbol{E}$ of circularly polarised (cp) light, and mediated by the Rosenfeld tensor (see section 2). Here $\boldsymbol{E}^*$ and $\boldsymbol{B}^*$ denote the complex conjugates of $\boldsymbol{E}$ and $\boldsymbol{B}$. The energy (4) corresponds to the real torque

$$\boldsymbol{T} = \tfrac{1}{2}\boldsymbol{\mu}^{(\mathrm{ind})} \times \boldsymbol{E}^* + \tfrac{1}{2}\boldsymbol{m}^{(\mathrm{ind})} \times \boldsymbol{B}^* + \mathrm{c.c.} \qquad (5)$$

In section 3 a description is given of the molecular dynamics (md) simulation method in the transient and field applied steady states for torques of type (5) generated by the interaction of right and left cp lasers with (S)-CHBrClF. The FMD method generates RTs and difference CFs. The FMD method is checked with a torque of type (5) applied to an ensemble of water molecules with right and left cp laser fields, using the surviving off-diagonal elements [56] of the Rosenfeld tensor in the C_{2v} water molecule. Section 4 presents results for: (a) the chiral and (b) the achiral molecular ensembles in terms of analytical Kielich functions [57] from energy terms of type (4); rise transients, and laser applied difference CFs which are pseudoscalars, and describe in statistical terms the different molecular dynamical effects of left and right cp laser radiation. The difference CF of molecular rotational velocity [58] is presented as the first evidence for the existence of ORD and CD in the far infrared.

In the achiral water ensemble, the difference CFs vanish in the noise of the FMD simulation, a result which is consistent with the fact that CD and ORD in water vanish in the absence of parity non-conservation [59]. However, the FMD method shows the existence of a novel anisotropy due to the non-zero off-diagonal elements in water of the Rosenfeld tensor. These elements generate a Kielich function, whose analytical form is found to be in detailed agreement with its FMD counterpart, constructed from saturation levels of rise transients.

Finally, the paper discusses possible experimental routes to far infrared CD and ORD, and likely extensions of the FMD technique to frequency dependent Rosenfeld tensor elements.

2. Development of the torque for right and left circularly polarised laser radiation

Consider a right or left circularly polarised laser propagating in the Z axis of the laboratory frame (X, Y, Z) through an ensemble of chiral molecules (an enantiomer). The electric and magnetic field components of the right (R) and left (L) electromagnetic plane waves are

$$\begin{aligned}
\boldsymbol{E}_{\mathrm{L}} &= E_0(\boldsymbol{e}_X + \mathrm{i}\boldsymbol{e}_Y)\exp(-\mathrm{i}\phi_{\mathrm{L}})\,, \\
\boldsymbol{E}_{\mathrm{R}} &= E_0(\boldsymbol{e}_X - \mathrm{i}\boldsymbol{e}_Y)\exp(-\mathrm{i}\phi_{\mathrm{R}})\,, \\
\boldsymbol{B}_{\mathrm{L}} &= B_0(-\mathrm{i}\boldsymbol{e}_X + \boldsymbol{e}_Y)\exp(-\mathrm{i}\phi_{\mathrm{L}})\,, \\
\boldsymbol{B}_{\mathrm{R}} &= B_0(\mathrm{i}\boldsymbol{e}_X + \boldsymbol{e}_Y)\exp(-\mathrm{i}\phi_{\mathrm{R}})\,,
\end{aligned} \qquad (6)$$

where $\boldsymbol{e}_X$ and $\boldsymbol{e}_Y$ are unit vectors in the X and Y axes of the laboratory frame (X, Y, Z). Here E_0 and B_0 are scalar electric and magnetic field amplitudes and ϕ_{L} and ϕ_{R} are left and right phases

$$\begin{aligned}
\phi_{\mathrm{L}} &= \omega t - |\boldsymbol{\kappa}_{\mathrm{L}}|Z\,, \\
\phi_{\mathrm{R}} &= \omega t - |\boldsymbol{\kappa}_{\mathrm{R}}|Z\,,
\end{aligned} \qquad (7)$$

where $\boldsymbol{\kappa}_{\mathrm{L}}$ and $\boldsymbol{\kappa}_{\mathrm{R}}$ are left and right wave vectors, ω is the angular frequency of the wave at an instant t and position $\boldsymbol{r}$.

The total torque mediated by the Rosenfeld tensor must be calculated from two processes (eq. (5)): (1) induction of a molecular electric dipole moment by the magnetic field of the electromagnetic plane wave, and (2) induction of a molecular magnetic dipole moment by its electric field

$$\mu_i^{\mathrm{ind}} = {}^{e}\alpha_{ij}^{m} B_j\,, \qquad (8)$$

$$m_i^{\mathrm{ind}} = {}^{m}\alpha_{ij}^{e} E_j\,. \qquad (9)$$

The polarizability tensor ${}^{m}\alpha_{ij}^{e}$ can be split similarly to (1)–(3) using the basic properties of ${}^{e}\alpha_{ij}^{m}$ [3, 6]:

$${}^{e}\beta_{ij}^{m} = {}^{m}\beta_{ji}^{e}\,, \qquad {}^{e}\beta_{ij}^{m\prime} = {}^{m}\beta_{ji}^{e\prime}\,, \qquad (10)$$

$${}^{e}\gamma_{ij}^{m} = -{}^{m}\gamma_{ji}^{e}\,, \qquad {}^{e}\gamma_{ij}^{m\prime} = -{}^{m}\gamma_{ji}^{e\prime}\,. \qquad (11)$$

The total torque experienced by the molecule is the real part of the expression

$$T_l = +\epsilon_{lij}({}^{e}\alpha^{m}_{ik} B_k E^*_j + {}^{m}\alpha^{e}_{ik} E_k B^*_j) . \tag{12}$$

It is well known from semi-classical theory [3] that both ORD and CD depend only on the diagonal components of ${}^{e}\hat{\boldsymbol{\gamma}}^{m}$ and ${}^{m}\boldsymbol{\gamma}^{e}$, which near optical resonance themselves become complex. The torque, a purely real quantity, must therefore be developed through products such as

$$T^{(1)}_l = -\epsilon_{lij}\,{}^{e}\gamma^{m}_{ik}\,\mathrm{Im}(E^*_j B_k) , \tag{13}$$

$$T^{(2)}_l = -\epsilon_{lij}\,{}^{m}\gamma^{e}_{ik}\,\mathrm{Im}(E_k B^*_j) . \tag{14}$$

The torque (13) is that between the induced electric dipole moment (8) and the electric field of the plane wave, the torque (14) is that between the induced magnetic dipole moment (9) and the magnetic field of the wave. The total torque is the sum of (13) and (14) ($\boldsymbol{T} = \boldsymbol{T}^{(1)} + \boldsymbol{T}^{(2)}$). Clearly, it is also possible to construct a purely real torque from the polarisability ${}^{e}\gamma^{m'}_{ik}$ and $\mathrm{Re}(E^*_j B_k)$ (and ${}^{m}\gamma^{e'}_{ik}$ and $\mathrm{Re}(E_k B^*_j)$) but this latter kind of torque is the same for right and left circularly polarised light, and cannot contribute to the effect simulated in this paper.

For circularly polarised light [6] the following relations are fulfilled:

$$\mathrm{Im}(E_k B^*_j)^{\mathrm{L}} = -\mathrm{Im}(E^*_j B_k)^{\mathrm{L}} , \tag{15}$$

$$\mathrm{Im}(E_k B^*_j)^{\mathrm{R}} = -\mathrm{Im}(E^*_j B_k)^{\mathrm{R}} , \tag{16}$$

$$\mathrm{Im}(E_k B^*_j)^{\mathrm{L}} = -\mathrm{Im}(E_k B^*_j)^{\mathrm{R}} , \tag{17}$$

which lead to the total torque

$$T^{\mathrm{L}}_l = -T^{\mathrm{R}}_l = -\epsilon_{lij}({}^{m}\gamma^{e}_{ik} + {}^{m}\gamma^{e}_{ki})\,\mathrm{Im}(E_k B^*_j)^{\mathrm{L}} . \tag{18}$$

It is convenient at this point to develop eq. (18) in terms of diagonal and off-diagonal elements of ${}^{m}\gamma^{e}_{ik}$ and to express both types in the frame (1, 2, 3) of the molecular point group. (Later we shall make use of this classification in the C_1 point group of (S)-CHBrClF and the C_{2v} point group of the water molecule.) The torque (18) given in the molecular frame

$$\begin{aligned} T^{\mathrm{L}}_l &= -T^{\mathrm{R}}_l \\ &= -\epsilon_{lij}({}^{m}\gamma^{e}_{ik} + {}^{m}\gamma^{e}_{ki})(e_{jX}e_{kX} + e_{jY}e_{kY})E_0 B_0 , \end{aligned} \tag{19}$$

where e_{jX}, for example, means the Xth laboratory frame component of the unit vector $\boldsymbol{e}_j$ fixed in the j axis of the frame (1, 2, 3). (In eq. (19), i, j, and k can take the values 1, 2, and 3.)

2.1. *Contribution of diagonal elements of ${}^{m}\boldsymbol{\gamma}^{e}$ to the torque*

The contribution to the torque (19) from diagonal elements of the polarisability tensor ${}^{m}\boldsymbol{\gamma}^{e}$ is

$$\begin{aligned} T^{\mathrm{L}}_1 &= -T^{\mathrm{R}}_1 \\ &= -2({}^{m}\gamma^{e}_{22} - {}^{m}\gamma^{e}_{33})(e_{2X}e_{3X} + e_{2Y}e_{3Y})E_0 B_0 , \\ T^{\mathrm{L}}_2 &= -T^{\mathrm{R}}_2 \\ &= -2({}^{m}\gamma^{e}_{33} - {}^{m}\gamma^{e}_{11})(e_{3X}e_{1X} + e_{3Y}e_{1Y})E_0 B_0 , \\ T^{\mathrm{L}}_3 &= -T^{\mathrm{R}}_3 \\ &= -2({}^{m}\gamma^{e}_{11} - {}^{m}\gamma^{e}_{22})(e_{1X}e_{2X} + e_{1Y}e_{2Y})E_0 B_0 . \end{aligned} \tag{20}$$

In eq. (20) the contribution from both torques (13) and (14) are exactly the same.

2.2. *Off-diagonal elements of ${}^{m}\boldsymbol{\gamma}^{e}$ in the torque*

From the general equation (19) we can develop the contribution to the total torque in the molecular frame from off-diagonal elements

$$\begin{aligned} T^{\mathrm{L}}_1 = -T^{\mathrm{R}}_1 = -[&({}^{m}\gamma^{e}_{12} + {}^{m}\gamma^{e}_{21})(e_{3X}e_{1X} + e_{3Y}e_{1Y}) \\ &-({}^{m}\gamma^{e}_{31} + {}^{m}\gamma^{e}_{13})(e_{1X}e_{2X} + e_{1Y}e_{2Y}) \\ &+({}^{m}\gamma^{e}_{23} + {}^{m}\gamma^{e}_{32})(e^2_{2Z} - e^2_{3Z})]E_0 B_0 , \\ T^{\mathrm{L}}_2 = -T^{\mathrm{R}}_2 = -[&({}^{m}\gamma^{e}_{23} + {}^{m}\gamma^{e}_{32})(e_{1X}e_{2X} + e_{1Y}e_{2Y}) \\ &-({}^{m}\gamma^{e}_{12} + {}^{m}\gamma^{e}_{21})(e_{2X}e_{3X} + e_{2Y}e_{3Y}) \\ &+({}^{m}\gamma^{e}_{31} + {}^{m}\gamma^{e}_{13})(e^2_{3Z} - e^2_{1Z})]E_0 B_0 , \end{aligned}$$

$$T_3^{\mathrm{L}} = -T_3^{\mathrm{R}} = -[({}^m\gamma_{31}^e + {}^m\gamma_{13}^e)(e_{2X}e_{3X} + e_{2Y}e_{3Y}) - ({}^m\gamma_{23}^e + {}^m\gamma_{32}^e)(e_{3X}e_{1X} + e_{3Y}e_{1Y}) + ({}^m\gamma_{12}^e + {}^m\gamma_{21}^e)(e_{1Z}^2 - e_{2Z}^2)]E_0B_0 , \quad (21)$$

The contributions to the "off-diagonal" torque (21) from the torques (13) and (14) are in general different except when off-diagonal elements of ${}^m\gamma_{ik}^e$ fulfill the relation ${}^m\gamma_{ik}^e = {}^m\gamma_{ki}^e$ in the molecular point group S_4 (see table A.1 of the appendix).

2.3. *Torque and molecular point group symmetry*

The total torque due to the ORD polarisability ${}^m\gamma_{ij}^e$ is the sum of diagonal and off-diagonal contributions (eqs. (20) and (21)). The number of independent contributing scalar elements is determined [3, 6] by the molecular point group. In this paper we consider the C_1 symmetry of (S)-CHBrClF and the C_{2v} symmetry of the water molecule. In the C_1 point group all nine elements of ${}^m\gamma_{ij}^e$ are in general non-zero and independent, but in the C_{2v} point group, if axis 1 labels that of the permanent electric dipole moment, we have

$${}^m\gamma_{23}^e \neq {}^m\gamma_{32}^e . \quad (22)$$

Equation (22) shows that even in an achiral molecule, there may be non-zero elements of the ORD and CD polarisabilities, something which is frequently overlooked. This means that in water there is a non-zero torque due to the Rosenfeld tensor, and this defines a Kielich function, second order rise transients, and anisotropy related to bi-axial birefringence. This apparently new phenomenon is simulated in this paper by FMD. It is well known experimentally, however, that there is no CD and ORD in water, so that this non-vanishing torque mediated by the Rosenfeld tensor cannot produce pseudoscalar phenomena [60, 61] such as rotation of the plane of polarisation of a linearly polarised probe laser, and cannot produce pseudoscalar difference CFs. This is corroborated in the FMD simulation. The Rosenfeld torque in water produces only bi-axial birefringence, i.e. a difference in refractive index in the propagation axis of the laser and orthogonal Cartesian axes. This is a scalar, not a pseudoscalar, observable. Clearly, this conclusion is consistent with the fact [3] that a pseudoscalar observable is supported only in chiral ensemble in the absence of parity non-conservation, and it is important to note that all difference CFs are also pseudoscalar observables, one of which, the rotational velocity difference CF, signifies the existence of far infrared ORD and CD.

3. FMD simulation methods

The FMD method used in this paper is based on the code TETRA, which is listed in full in the the literature [62], and which has been animated for video casette [63, 64]. TETRA is a robust and widely used algorithm which produces a variety of thermodynamic and dynamical information. The total torque (20) plus (21) was coded into the forces loop [14–23], and second order rise transients of the type

$$\langle e_{1Z}^2 \rangle, \langle e_{2Z}^2 \rangle, \langle e_{3Z}^2 \rangle , \ldots$$

monitored until saturation both for (S)-CHBrClF and for water.

3.1. *(S)-CHBrClF*

The intermolecular potential is a site-site Lennard-Jones type first reported in [65]:

$$\phi_{ij} = 4\sum_{i,j}\epsilon\left[\left(\frac{\sigma}{r_{ij}}\right)^{12} - \left(\frac{\sigma}{r_{ij}}\right)^{6}\right] + \text{charge–charge} , \quad (23)$$

$\epsilon/k(\mathrm{H–H}) = 10.0\ \mathrm{K}$, $\sigma(\mathrm{H–H}) = 2.8\ \text{Å}$,
$\epsilon/k(\mathrm{C–C}) = 35.8\ \mathrm{K}$, $\sigma(\mathrm{C–C}) = 3.4\ \text{Å}$,
$\epsilon/k(\mathrm{F–F}) = 54.9\ \mathrm{K}$, $\sigma(\mathrm{F–F}) = 2.7\ \text{Å}$,
$\epsilon/k(\mathrm{Cl–Cl}) = 158.0\ \mathrm{K}$, $\sigma(\mathrm{Cl–Cl}) = 3.6\ \text{Å}$,
$\epsilon/k(\mathrm{Br–Br}) = 218.0\ \mathrm{K}$, $\sigma(\mathrm{Br–Br}) = 3.9\ \text{Å}$,
$q(\mathrm{H}) = 0.225|e|$, $q(\mathrm{C}) = 0.335|e|$,
$q(\mathrm{F}) = -0.22|e|$, $q(\mathrm{Cl}) = -0.18|e|$,
$q(\mathrm{Br}) = -0.16|e|$.

A time step of 5.0 fs was used to integrate the equations of motion for 108 molecules. Isotropy in the liquid state in the laser off condition (field free equilibrium) was monitored through the fact that second order orientational averages fluctuate about the value $\frac{1}{3}$, fourth order about $\frac{1}{5}$, and so on for X, Y, and Z components of the unit vectors $\boldsymbol{e}_1$, $\boldsymbol{e}_2$, and $\boldsymbol{e}_3$ in frame $(1,2,3)$. First, third, fifth, etc. order orientational averages vanish. Frame $(1,2,3)$ was defined as the frame of the principal molecular moments of inertia [65]. Therefore, at field free equilibrium

$$\langle e_{1Z}^2 \rangle = \langle e_{2Z}^2 \rangle = \langle e_{3Z}^2 \rangle = \tfrac{1}{3} ,$$
$$\langle e_{1Z}^4 \rangle = \langle e_{2Z}^4 \rangle = \langle e_{3Z}^4 \rangle = \tfrac{1}{5} , \qquad (24)$$

and so on.

Following the application of torque (20) plus torque (21), rise transients for a laser propagating in the Z axis of the laboratory frame were monitored until saturation, using up to 4000 time steps. The development of anisotropy through second order orientational rise transients is exemplified in fig. 1 both for left and right cp lasers. For the same molecular trajectories, it was observed that all first order transients fluctuated around a mean value of zero. In computing the curves of fig. 1, the following nine scalar elements were used of the ORD polarisability, in the apparent absence of ab initio or experimental data:

$$^m\gamma_{11}^e : {}^m\gamma_{22}^e : {}^m\gamma_{33}^e : {}^m\gamma_{12}^e : {}^m\gamma_{13}^e : {}^m\gamma_{21}^e :$$
$$^m\gamma_{23}^e : {}^m\gamma_{31}^e : {}^m\gamma_{32}^e$$
$$= 7 : 8 : 9 : 1 : 2 : 3 : 4 : 5 : 6 . \qquad (25)$$

Changing these numbers will clearly change the details of the time dependence of the transients in fig. 1, but not the following fundamentals:
(1) The saturation values of the transients are different for left and right cp radiation.

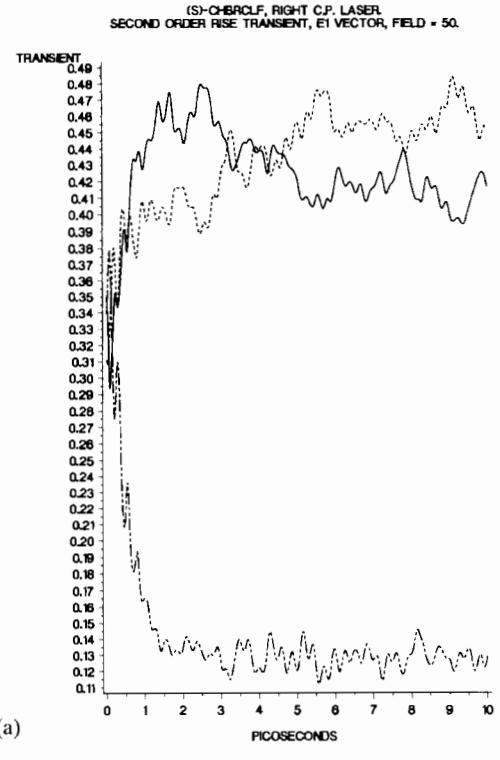

(a)

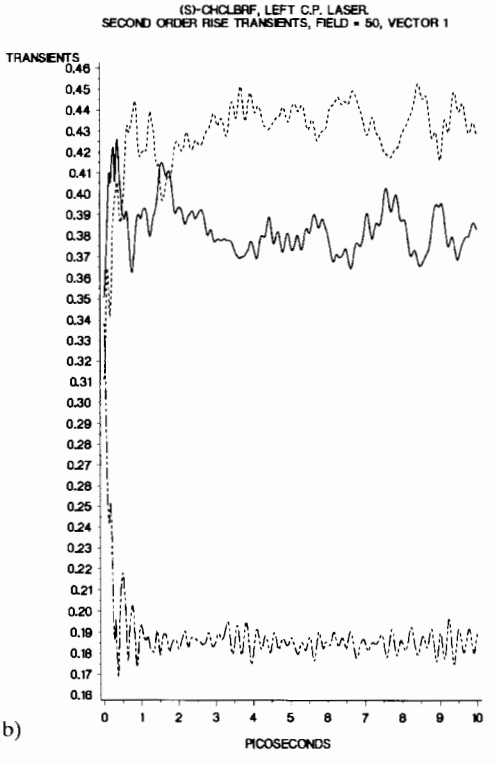

(b)

Fig. 1. Second order rise transients for liquid (S)-CHBrClF: (a) right; (b) left cp plane wave propagating through the sample in the Z axis of the laboratory frame. ——, $\langle e_{1X}^2 \rangle$; -------, $\langle e_{1Y}^2 \rangle$; – · · – · · – · · –, $\langle e_{1Z}^2 \rangle$.

(2) The time dependencies of the transients in the pre-saturation inverval are also different.

The feature (1) implies immediately that the Kielich functions of CD and ORD should be different for right and left cp radiation using a given enantiomer, and later in this paper, this is confirmed by an independent method based on thermodynamic averaging. This method and FMD agree in detail, Kielich functions for CD and ORD being constructed by plotting saturation levels such as those in fig. 1 against the interaction energy per molecule.

An idea of the effect of the cp laser on the potential energy of the sample was obtained by computing over up to 6000 time steps the configurational part of the internal potential energy of the ensemble ($\langle U \rangle$), both in the presence and absence of the applied electromagnetic plane wave:

$$\langle U \rangle = \left\langle \sum_{i<j} \sum \phi_{ij} \right\rangle + U_c \,, \tag{26}$$

here the sum is over all atom–atom pairs for which the interatomic distance r_{ij} is less than the cut-off distance r_c of the potential. The correction U_c is based on a uniform distribution of the molecules beyond this cut-off distance [62].

In the FMD computation of transients [14], a numerical thermostatting routine is necessary to maintain the mean translational and rotational temperature of the sample near the input values (both 296 K). When the laser is applied to the sample (i.e. when the torque is switched on at an instant t) there is an immediate increase in temperature and pressure, because energy is being pumped in to a finite molar volume, which is fixed in constant volume magnetic dipole simulation [66]. The temperature rescaling routine drives down the rotational and translational temperature towards the input value (296 K) by rescaling the kinetic energies every N time steps, where N is an input parameter. Since temperature is kinetic energy this means that the linear and angular velocity vectors are scaled back every N steps. Animations [63, 64] show directly that the effect is to cause jumps in the absolute values of these vectors for individual molecules, leaving all 108 vectors relatively unchanged. There is no discernible visual effect [63, 64] on the orientation vectors. The RTs for this work and is related FMD simulations [42] of the frequency doubled optical Stark effect were computed with $N = 50$, and occasionally checked with $N = 1$. The saturation levels reached by the transients are unaffected within the noise by replacing $N = 50$ by $N = 1$, but rescaling every time step tends to eliminate rise transient oscillations (these are not discontinuities), and an example of this is given in ref. [42]. The change $N = 50$ to $N = 1$ has no discernible effect on the time taken to achieve saturation in the RT.

In the post saturation state, i.e. the laser applied stationary state, ACFs, and difference CFs were computed over 6000 time steps by running time averaging, and displayed to 400 time steps only, thus maintaining "good statistics" for each cartesian component of the CF. In this field-on condition, temperature rescaling every 50 time steps was considered adequate, and the difference CFs show no discontinuities due to rescaling. In this laser on condition, animations [63, 64] are available of related work on the inverse Zeeman effect, and reveal in direct detail the effect of the laser on the molecular dynamics. (These animations are currently available from MWE at his Cornell address, or from IBM. Reference [64] will shortly be distributed by Media Magic of California.)

Without digital rescaling , or thermostatting, the sample would heat up rapidly, causing a commensurate increase in pressure, until floating point overflow eventually stops the production run.

It is noteworthy, while on the subject of temperature rescaling, that whenever Langevin or Kielich functions are definable, the saturation levels of rise transients from FMD reproduce the functions in detail. This was one of the first checks [14] applied to the technique. Such a check is made later in this paper, and again, detailed agreement obtained.

3.2. Water

The FMD simulations for liquid water were carried out at 296 K and 1.0 bar with a time step

of 0.5 fs. The frame (1, 2, 3) was the frame of the principal molecular moments of inertia, with axis 1 labelled as that of the permanent electric dipole moment. The intermolecular potential is a modified ST2 first introduced in ref. [67]:

$$\phi_{ij} = 4\sum_{ij}\epsilon\left[\left(\frac{\sigma}{r_{ij}}\right)^{12} - \left(\frac{\sigma}{r_{ij}}\right)^{6}\right] + \text{charge–charge}\,, \tag{27}$$

$$\epsilon/k(\text{H–H}) = 21.1\ \text{K}\,, \qquad \sigma(\text{H–H}) = 2.25\ \text{Å}\,,$$

$$\epsilon/k(\text{O–O}) = 58.4\ \text{K}\,, \qquad \sigma(\text{O–O}) = 2.80\ \text{Å}\,,$$

$$a^q(\text{H}) = 0.23|e|\,, \qquad q(\text{O}) = 0.00|e|\,,$$

$$q\ (\text{partial charge}) = -0.23|e|\,.$$

This has been tested in detail against the flexible MCYL water potential [68] and against experimental data for water from 10 to 1273 K and several kilobar [69]. RTs and difference CFs were computed as described for the enantiomer (S)-CHBrClF, with a torque mediated by the ORD polarisability's surviving off diagonal elements, eq. (23), for several different values of

$$C_0 = E_0 B_0({}^m\gamma^e_{23} + {}^m\gamma^e_{32})\,, \tag{28}$$

so that a Kielich function was generated from FMD by plotting the saturation values of second order orientational RTs generated by this torque. For each value of the parameter C_0, the simulation was carried out with left and right cp laser radiation, and left and right RTs, ACFs, and difference CFs computed.

4. Results: comparison with Kielich functions, and far infrared ORD

The FMD transient results in fig. 1 show for the first time that OED (and by implication CD) is accompanied by Kielich functions which are different for right and left circularly polarised radiation. In the appendix the derivation of these Kielich functions is detailed both for (S)-CHBrClF and for water through the mediacy of the Rosenfeld tensor, giving expressions such as the following for the saturation levels of second order transients versus interaction energy per molecule.

4.1. (S)–CHBrClF

$$I_1 = \exp\Big[\mp q\Big(\cos^2\theta - \frac{h}{q}\sin^2\theta\cos 2\phi + \frac{a_1}{q}\sin\phi\sin\theta\cos\theta + \frac{a_2}{q}\cos\phi\sin\theta\cos\theta + \frac{a_3}{q}\sin\phi\cos\phi\sin^2\theta\Big)\Big]\,,$$

$$\langle e^2_{1Z}\rangle = \langle\cos^2\theta\rangle = \int_0^{\pi}\int_0^{2\pi}\cos^2\theta\sin\theta I_1\,\mathrm{d}\phi\,\mathrm{d}\theta \Big/ \int_0^{\pi}\int_0^{2\pi}\sin\theta I_1\,\mathrm{d}\phi\,\mathrm{d}\theta\,,$$

$$\langle e^2_{2Z}\rangle = \langle\sin^2\phi\sin^2\theta\rangle = \int_0^{\pi}\int_0^{2\pi}\sin^3\theta\sin^2\phi I_1\,\mathrm{d}\phi\,\mathrm{d}\theta \Big/ \int_0^{\pi}\int_0^{2\pi}\sin\theta I_1\,\mathrm{d}\phi\,\mathrm{d}\theta\,,$$

$$\langle e^2_{3Z}\rangle = \langle\cos^2\phi\sin^2\theta\rangle = \int_0^{\pi}\int_0^{2\pi}\sin^3\theta\cos^2\phi I_1\,\mathrm{d}\phi\,\mathrm{d}\theta \Big/ \int_0^{\pi}\int_0^{2\pi}\sin\theta I_1\,\mathrm{d}\phi\,\mathrm{d}\theta\,,$$

$$d = {}^m\gamma^e_{11} - \tfrac{1}{2}({}^m\gamma^e_{22} + {}^m\gamma^e_{33})\,, \qquad q = \frac{dE_0^2}{ckT}\,,$$

$$\frac{h}{q} = \frac{{}^m\gamma^e_{22} - {}^m\gamma^e_{33}}{2d}\,, \quad \frac{a_1}{q} = \frac{{}^m\gamma^e_{12} + {}^m\gamma^e_{21}}{d}\,,$$

$$\frac{a_2}{q} = \frac{{}^m\gamma^e_{13} + {}^m\gamma^e_{31}}{d}\,, \quad \frac{a_3}{q} = \frac{{}^m\gamma^e_{23} + {}^m\gamma^e_{32}}{d}\,.$$

Here θ and ϕ denote the Euler angles, and other parameters are defined through individual scalar elements of the ORD polarisability for C_1 (chiral) symmetry (see the appendix). The upper sign (−) is related to right and the lower sign (+) to left cp light. For water, the corresponding expressions are as follows.

4.2. Water

$$\langle e_{1Z}^2 \rangle = \langle \cos^2 \theta \rangle = \frac{\int_0^{\pi}\int_0^{2\pi} \cos^2\theta \sin\theta I_2 \, d\phi \, d\theta}{\int_0^{\pi}\int_0^{2\pi} \sin\theta I_2 \, d\phi \, d\theta},$$

$$\langle e_{2Z}^2 \rangle = \langle \sin^2\phi \sin^2\theta \rangle = \frac{\int_0^{\pi}\int_0^{2\pi} \sin^3\theta \sin^2\phi I_2 \, d\phi \, d\theta}{\int_0^{\pi}\int_0^{2\pi} \sin\theta I_2 \, d\phi \, d\theta}, \qquad (30)$$

$$\langle e_{3Z}^2 \rangle = \langle \cos^2\phi \sin^2\theta \rangle = \frac{\int_0^{\pi}\int_0^{2\pi} \sin^3\theta \cos^2\phi I_2 \, d\phi \, d\theta}{\int_0^{\pi}\int_0^{2\pi} \sin\theta I_2 \, d\phi \, d\theta},$$

$$I_2 = \exp(\mp a \sin\phi \cos\phi \sin^2\theta),$$

$$a = \frac{({}^m\gamma_{23}^e + {}^m\gamma_{32}^e)E_0^2}{ckT}.$$

Both types of double integral are analytically intractable, and were integrated using a double Gauss–Legendre quadrature routine DGLNQ2 from the IBM numerical library of the IBM 3090-6S supercomputer of ETH, Zurich. The integration grid was 48×48, with a few checking runs at 24×24 to monitor for any numerical instabilities.

For (S)-CHBrClF, the change from right circular polarisation to left is accounted for in the Kielich functions (29) by changing the sign of the parameter q from negative to positive. The same thing is accomplished for the water Kielich functions (30) by changing the sign of parameter a. The results obtained from these two numerical quadratures are compared against the saturation levels of a number of FMD transients in figs. 2 and 3. For the second order transients

$$\langle e_{1Z}^2 \rangle, \quad \langle e_{2Z}^2 \rangle, \quad \langle {}^2_{3Z} \rangle,$$

satisfactory and detailed agreement is obtained between FMD and the Kielich functions across the complete range of existence. For (S)-CHBrClF, both FMD and numerical quadrature produce different Kielich functions by switching from right to left circular polarisation. In FMD, the switch is accomplished by changing the sign of the coded total torque, in the quadrature, the sign of q is changed. For all three unit vectors, figs. 2 and 3 show clearly that these two totally independent methods agree closely within the numerical uncertainties inherent in both. In FMD, uncertainty bars are generated by the noise level of the saturated second order transient (fig. 1), and there is also numerical uncertainty in the double quadrature. An example of this can be seen in fig. 2 at the point $q = 0$, where the theoretical value of the double integral should be $\frac{1}{3}$. The routine DGLNG2 reproduces this to within about ± 0.01, but the quadrature result for $\langle e_{3Z}^2 \rangle$ is systematically slightly too low, and that for $\langle e_{1Z}^2 \rangle$ is slightly too high due purely to the numerical uncertainty in the double Gauss–Legendre quadrature with 48×48 grid. As q becomes smaller in figs. 2(a) and (b) the FMD uncertainty grows, because the noise in the saturation level of the second order transients is greater. The parameters used for the ORD polarisability were the same in both methods, the arbitrary sequence described in section 3.

For water, fig. 3, detailed agreement is again obtained with both methods, but changing the sign of the parameter a does not affect the Kielich function within the uncertainties, showing that in the achiral water molecule, the Rosenfeld tensor produces a novel scalar bi-axial anisotropy, but does not produce a pseudoscalar optical rotation. In this context it is interesting to note that the difference between the left and right Kielich functions for (S)-CHBrClF is a pseudoscalar.

The FMD method has therefore been used successfully to describe the Kielich functions for ORD and CD.

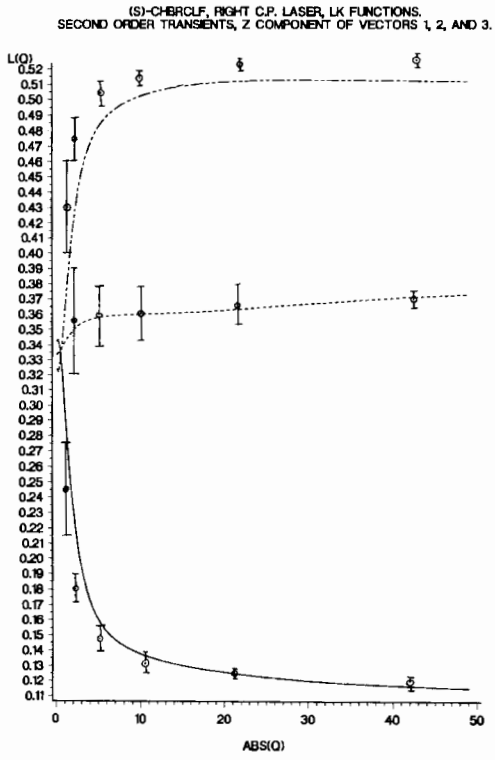

(a)

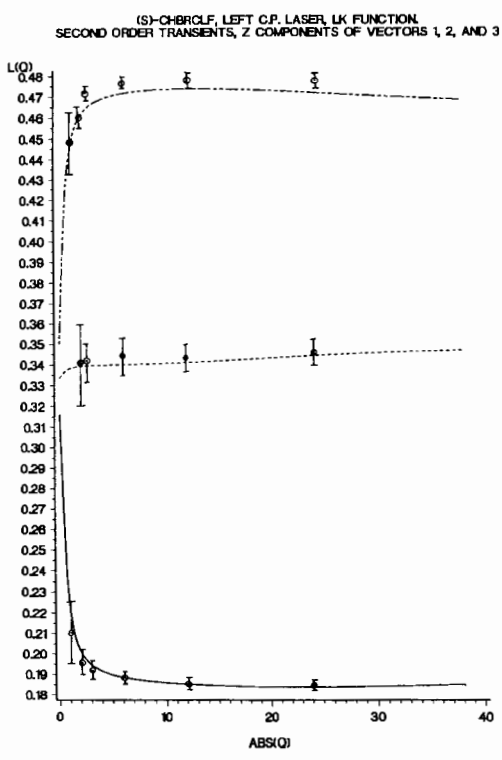

(b)

Fig. 2. Comparison of Kielich functions for (S)-CHBrClF from FMD (points with uncertainty bars) and eqs. (29) (lines). ——, $\langle e_{1Z}^2 \rangle$; ------, $\langle e_{2Z}^2 \rangle$; – · · – · · –, $\langle e_{3Z}^2 \rangle$. (a) right; (b) left cp plane waves propagating in axis Z. Plotted as functions of $|q|$.

It is now possible to proceed with a degree of confidence to investigate with FMD the picosecond scale molecular dynamics of the chiral and achiral ensembles. In particular, it is of immediate experimental interest to look for evidence for far infrared CD and ORD with the rotational velocity autocorrelation function

$$C_{1ij}(t) = \frac{\langle \dot{e}_{1i}(t)\dot{e}_{1j}(0)\rangle}{\langle \dot{e}_{1i}^2 \rangle^{1/2}\langle \dot{e}_{1j}^2 \rangle^{1/2}} \,. \tag{31}$$

This is essentially the Fourier transform of the far infrared power absorption coefficient [12], and was computed in this work as part of an extensive data bank of time correlation functions mediated by the Rosenfeld tensor both in (S)-CHBrClF and water. There is space here only for a representative sample of results.

4.3. (S)-CHBrClF

Difference CFs were computed for a number of applied laser intensities, measured through the parameter $E_0 B_0$ in eq. (18). Of direct interest to ORD are the results for the rotational velocity difference CF, defined by

$$C_{1\mathrm{diff}}(t) = \left[\frac{\langle \dot{e}_{1i}(t)\dot{e}_{1j}(0)\rangle}{\langle \dot{e}_{1i}^2 \rangle^{1/2}\langle \dot{e}_{1j}^2 \rangle^{1/2}} \right]_{\mathrm{L}} - \left[\frac{\langle \dot{e}_{1i}(t)\dot{e}_{1j}(0)\rangle}{\langle \dot{e}_{1i}^2 \rangle^{1/2}\langle \dot{e}_{1j}^2 \rangle^{1/2}} \right]_{\mathrm{R}} , \tag{32}$$

and whose real Fourier transform [12],

$$C_{1\mathrm{diff}}(\omega) = \int_0^\infty C_{1\mathrm{diff}}(t) \cos \omega t \, \mathrm{d}t \,, \tag{33}$$

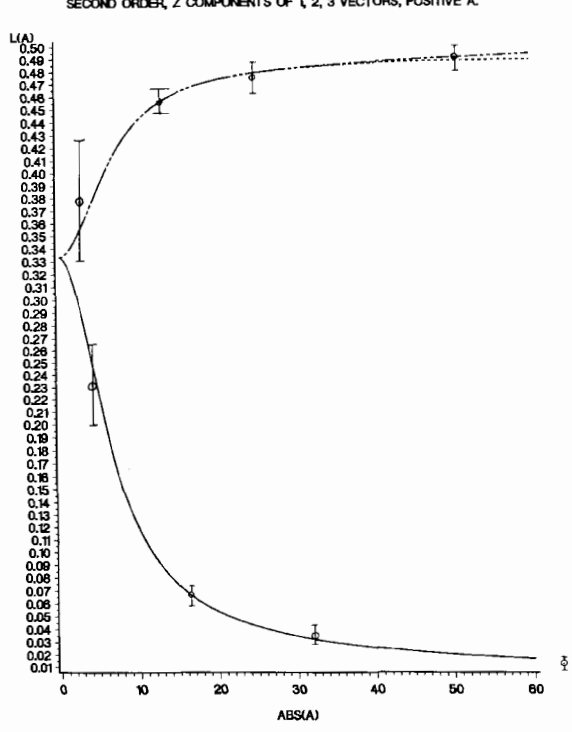

Fig. 3. As for fig. 2, Kielich functions for water plotted as a function of $|a|$.

in far infrared optical rotatory dispersion. The sequence in fig. 4 illustrates the behaviour of $C_{1\mathrm{diff}}(t)$ for increasing $E_0 B_0$ and is clear evidence for the existence of far infrared ORD. Note that $C_{1\mathrm{diff}}(t)$ is a time even pseudoscalar observable, and that the Z component has a different time dependence from those of the X and Y components. In arriving at the results of fig. 4 we have assumed implicitly that the ORD polarisability tensor ${}^{m}\gamma^{e}_{ij}$ is frequency independent (section 3), whereas more generally, the complex Rosenfeld tensor is well known [3] from perturbation theory to be frequency dependent. We return to this point in the discussion. Therefore the results in fig. 4 can give only an indication of the fundamentals of far infrared ORD, further progress being dependent on more detailed knowledge of ${}^{m}\alpha^{e}_{ij}(-\omega, \omega)$ in the far infrared range. However, fig. 4 reveals, importantly, that molecular dynamics computer simulation, in particular the FMD technique, is capable of demonstrating the different interactions between a given enantiomorph and left and right cp radiation in terms of fundamental molecular rotational and translational dynamics on a picosecond time scale. Furthermore, this has been achieved with a very small sample of 108 molecules over 6000 time steps.

The sequence of results in figs. 5 and 6 illustrate the difference CFs, respectively, of angular momentum and orientation, defined by

$$C_{2\mathrm{diff}}(t) = \left[\frac{\langle J_i(t) J_j(0) \rangle}{\langle J_i^2 \rangle^{1/2} \langle J_j^2 \rangle^{1/2}} \right]_{\mathrm{L}} - \left[\frac{\langle J_i(t) J_j(0) \rangle}{\langle J_i^2 \rangle^{1/2} \langle J_j^2 \rangle^{1/2}} \right]_{\mathrm{R}}, \tag{34}$$

and

$$C_{3\mathrm{diff}}(t) = \left[\frac{\langle e_{1i}(t) e_{1j}(0) \rangle}{\langle e_{1i}^2 \rangle^{1/2} \langle e_{1j}^2 \rangle^{1/2}} \right]_{\mathrm{L}} - \left[\frac{\langle e_{1i}(t) e_{1j}(0) \rangle}{\langle e_{1i}^2 \rangle^{1/2} \langle e_{1j}^2 \rangle^{1/2}} \right]_{\mathrm{R}}. \tag{35}$$

In figs. 4–6 the Z component clearly has a different time dependence from the X and Y components, indicating that ORD (and by implication CD) is accompanied by the development of anisotropy in the molecular rotation/translation dynamics. Another check of the FMD method is that X and Y components of the difference CFs in figs. 4–6 have the same time dependence within the uncertainty. This is expected by symmetry, because the electromagnetic plane wave propagates in the Z axis of the laboratory frame (X, Y, Z).

4.4. Water

For water, difference CFs of the type illustrated in figs. 4–6 vanish in the uncertainty, a result which is consistent with the fact that an achiral ensemble cannot support pseudo-scalar observables [60]. However, fig. 7 illustrates what we believe to be a novel anisotropy phenomenon due to the off-diagonal elements in water of the ORD polarisability ${}^{m}\gamma^{e}_{23} - {}^{m}\gamma^{e}_{32}$. This type of

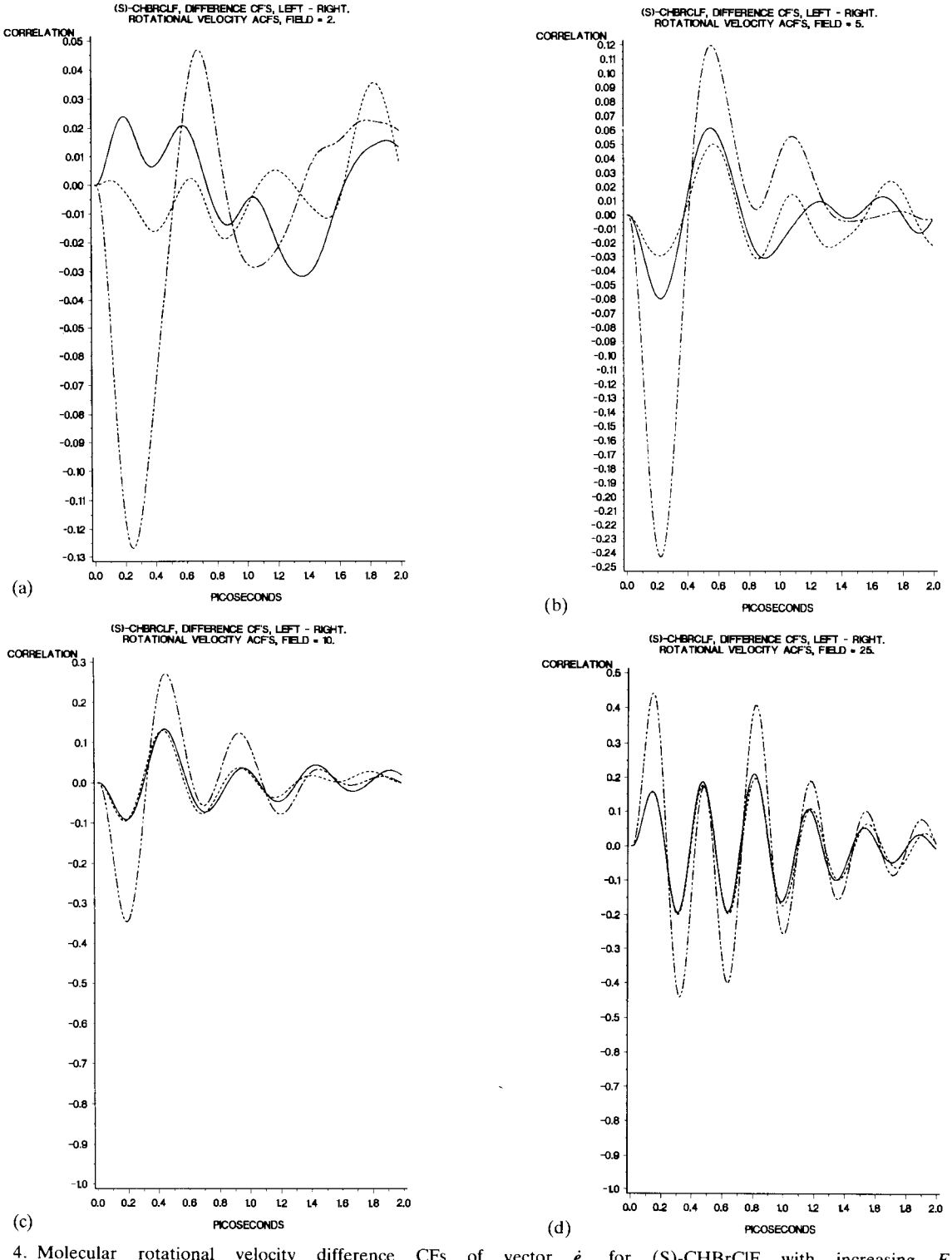

Fig. 4. Molecular rotational velocity difference CFs of vector $\dot{e}_1$ for (S)-CHBrClF with increasing E_0B_0. $(a):(b):(c):(d):(e):(f):(g) = 2:5:10:25:50:100:200$. ——, $i = j = X$; -------, $i = j = Y$; – · · – · · – · · –, $i = j = Z$.

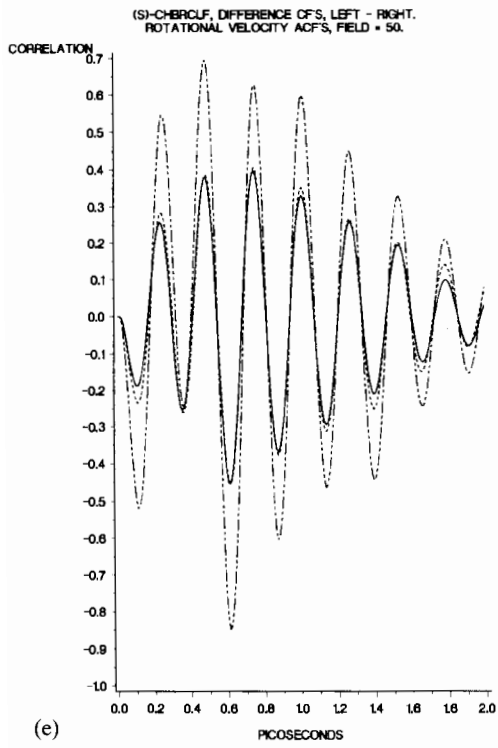

(e)

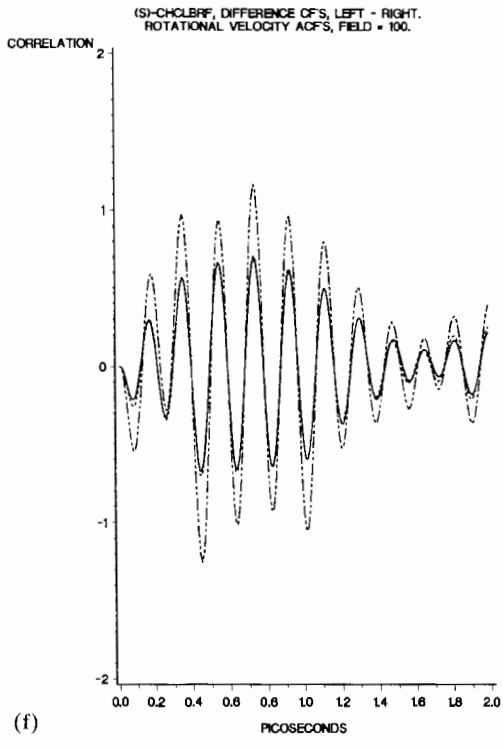

(f)

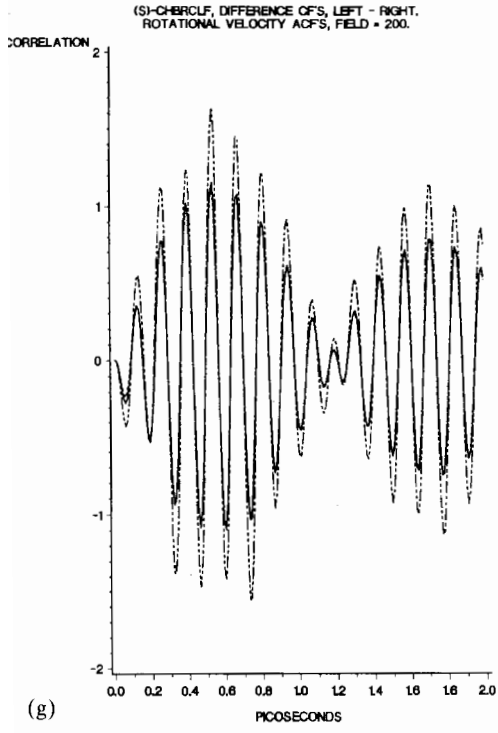

(g)

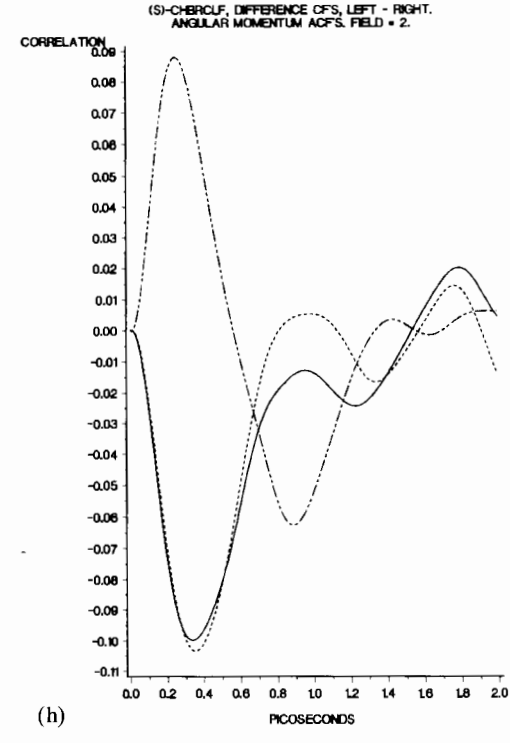

(h)

Fig. 4 (cont.).

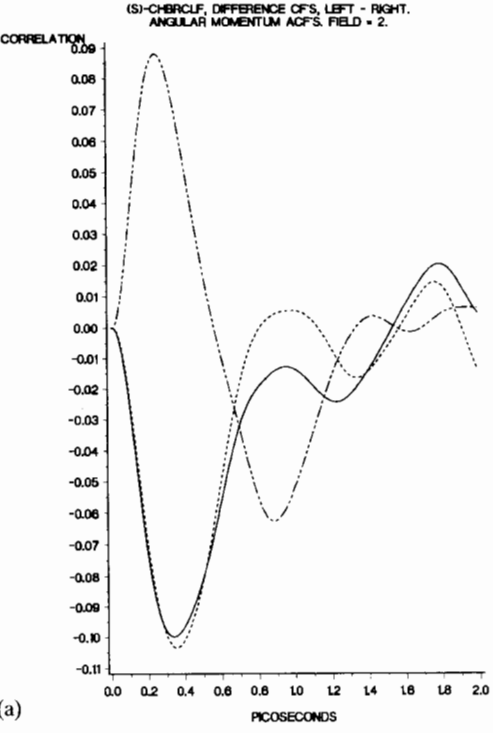

(a)

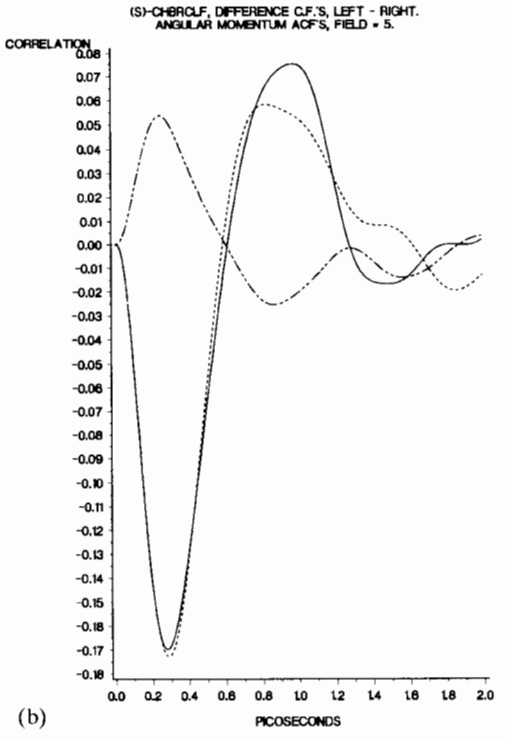

(b)

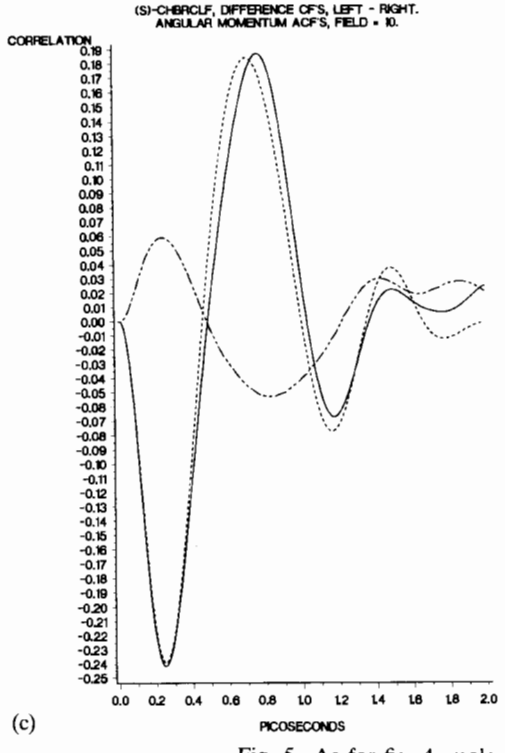

(c)

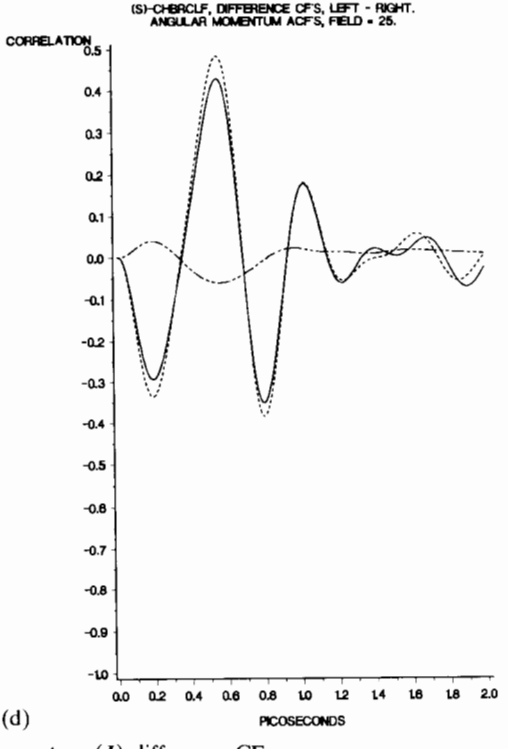

(d)

Fig. 5. As for fig. 4, molecular angular momentum (J) difference CFs.

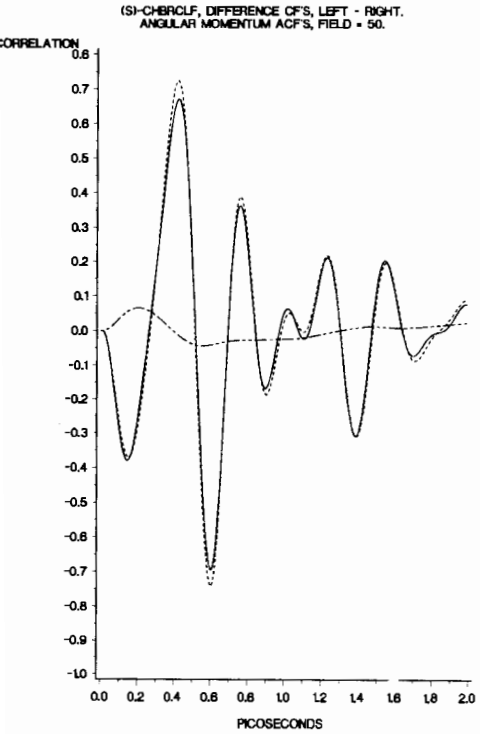
(S)-CHBRCLF, DIFFERENCE CF'S, LEFT - RIGHT.
ANGULAR MOMENTUM ACF'S, FIELD = 50.
CORRELATION
PICOSECONDS

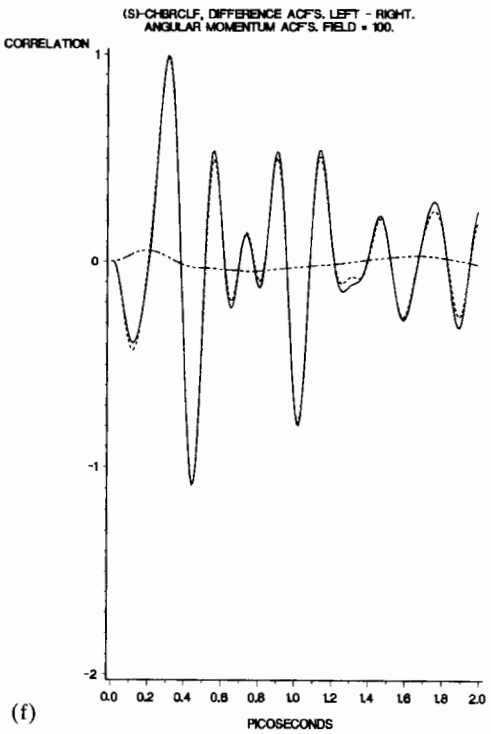
(S)-CHBRCLF, DIFFERENCE ACF'S. LEFT - RIGHT.
ANGULAR MOMENTUM ACF'S. FIELD = 100.
CORRELATION
PICOSECONDS

(f)

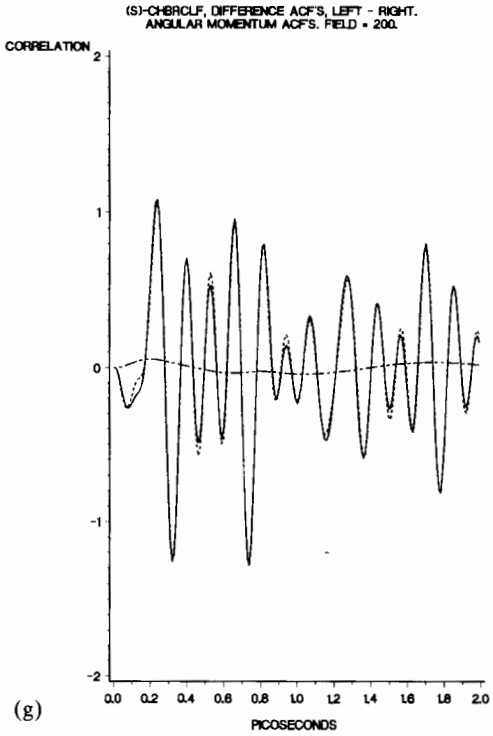
(S)-CHBRCLF, DIFFERENCE ACF'S, LEFT - RIGHT.
ANGULAR MOMENTUM ACF'S. FIELD = 200.
CORRELATION
PICOSECONDS

(g)

Fig. 5 (cont.).

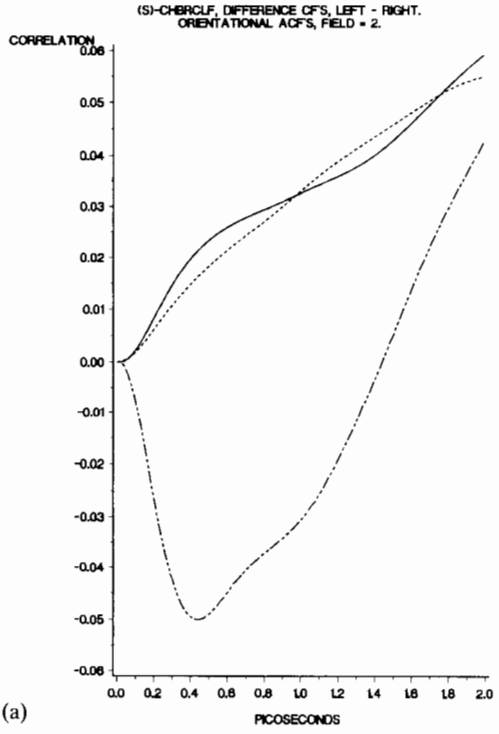

(a)

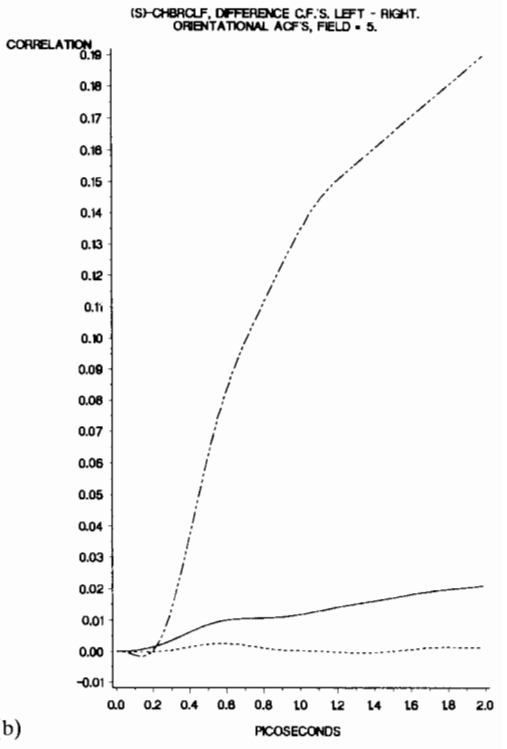

(b)

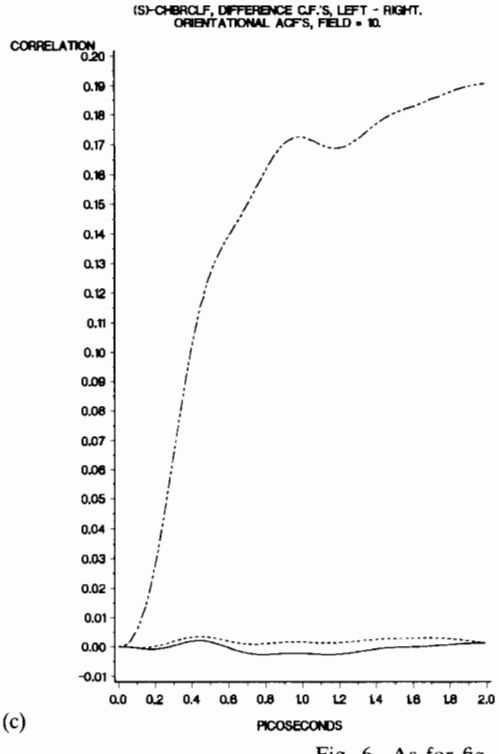

(c)

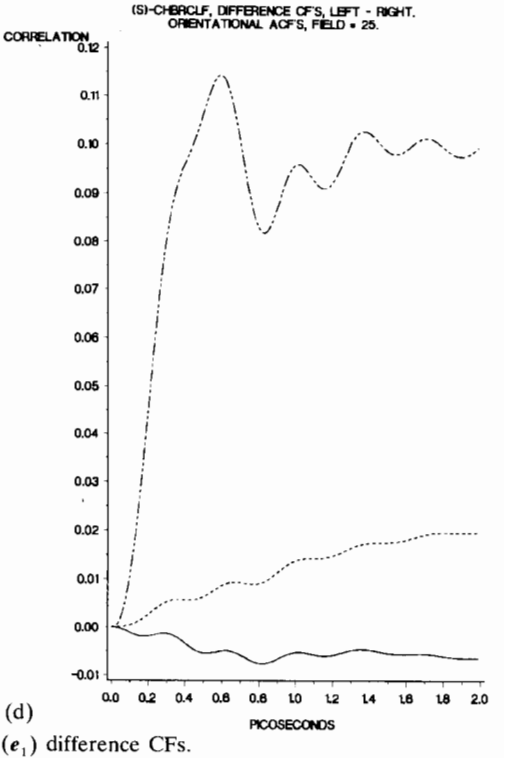

(d)

Fig. 6. As for fig. 5, orientational (e_1) difference CFs.

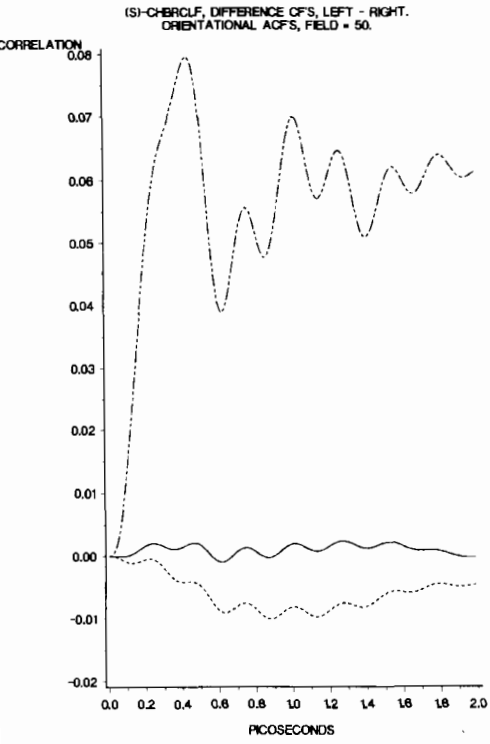
(S)-CHBRCLF, DIFFERENCE CF'S, LEFT - RIGHT.
ORIENTATIONAL ACF'S, FIELD = 50.
CORRELATION
0.08
0.07
0.06
0.05
0.04
0.03
0.02
0.01
0.00
-0.01
-0.02
0.0 0.2 0.4 0.6 0.8 1.0 1.2 1.4 1.6 1.8 2.0
PICOSECONDS

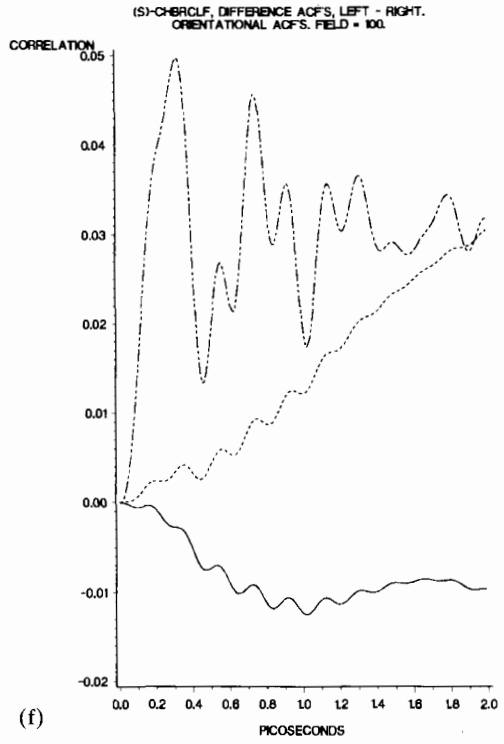
(S)-CHBRCLF, DIFFERENCE ACF'S, LEFT - RIGHT.
ORIENTATIONAL ACF'S, FIELD = 100.
CORRELATION
0.05
0.04
0.03
0.02
0.01
0.00
-0.01
-0.02
0.0 0.2 0.4 0.6 0.8 1.0 1.2 1.4 1.6 1.8 2.0
PICOSECONDS

(f)

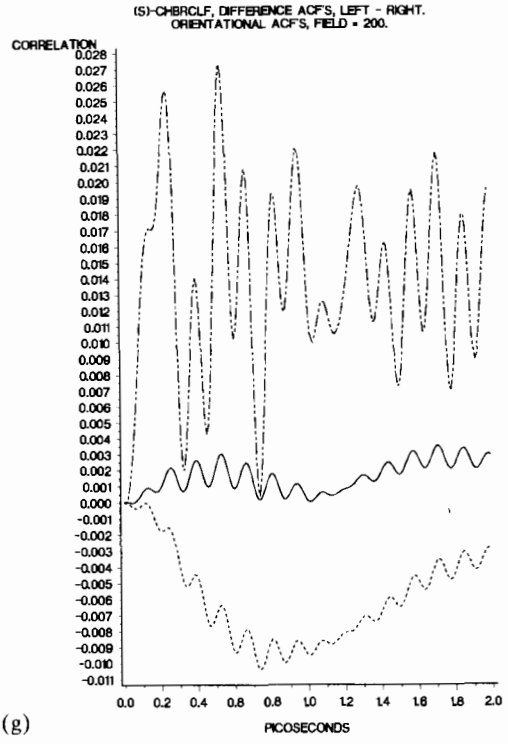
(S)-CHBRCLF, DIFFERENCE ACF'S, LEFT - RIGHT.
ORIENTATIONAL ACF'S, FIELD = 200.
CORRELATION
0.028
0.027
0.026
0.025
0.024
0.023
0.022
0.021
0.020
0.019
0.018
0.017
0.016
0.015
0.014
0.013
0.012
0.011
0.010
0.009
0.008
0.007
0.006
0.005
0.004
0.003
0.002
0.001
0.000
-0.001
-0.002
-0.003
-0.004
-0.005
-0.006
-0.007
-0.008
-0.009
-0.010
-0.011
0.0 0.2 0.4 0.6 0.8 1.0 1.2 1.4 1.6 1.8 2.0
PICOSECONDS

(g)

Fig. 6 (cont.).

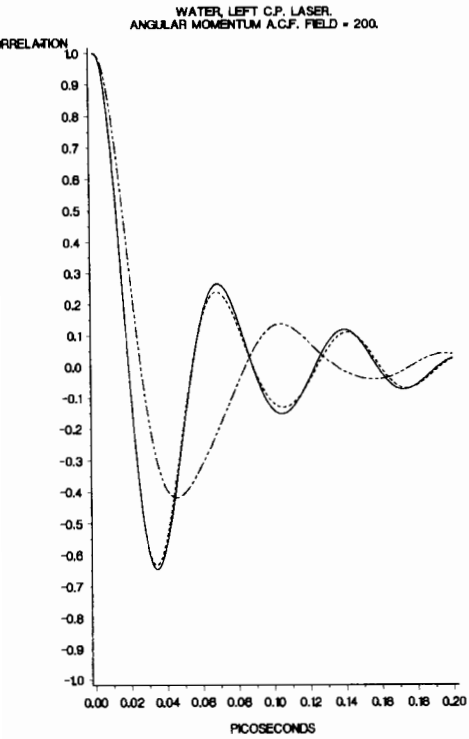

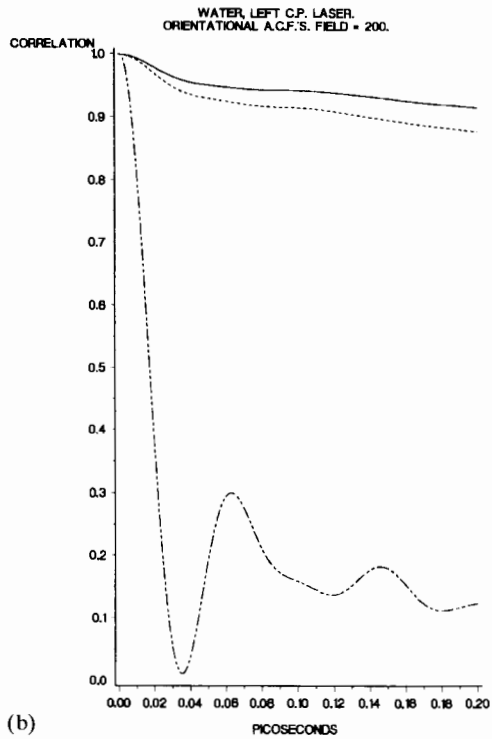

(b)

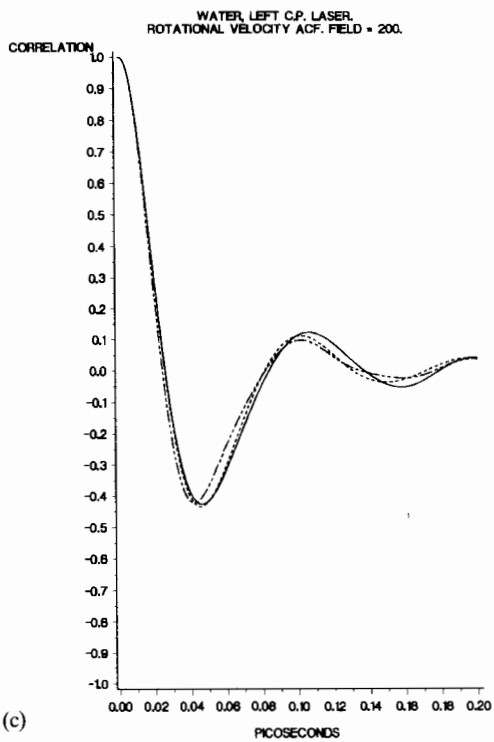

(c)

Liquid water, anisotropy due to ${}^{m}\gamma^{e}_{23} - {}^{m}\gamma^{e}_{32}$, the bi-axial Rosenfeld anisotropy. (a) Molecular angular momentum ACFs; olecular orientational ACFs ($\boldsymbol{e}_1$, the permanent molecular electric dipole moment unit vector); (c) molecular rotational y ACFs ($\dot{\boldsymbol{e}}_1$). ——, $i = j = X$; -------, $i = j = Y$; – · · – · · – · ·, $i = j = Z$.

anisotropy reveals itself clearly in fig. 7 in the angular momentum and orientational ACFs, and is also discernible in the rotational velocity ACF. In each case the $i = j = Z$ component of the ACF develops a different time dependence due to the influence of ${}^{m}\gamma^{e}_{ij}$, despite the fact that there is no ORD or CD. The anisotropy is the same for left and right cp plane waves, but vanishes in a plane polarised laser, where there are equal proportions of right and left cp components. It is concluded that when a cp laser interacts with the ${}^{m}\gamma^{e}_{ij}$ tensor, the refractive index in the direction of propagation of the laser becomes measurably different from those in the two orthogonal directions. This type of bi-axial (as distinct from circular) birefringence, is the same for left and right cp lasers, and vanishes for a plane polarised laser. These characteristics allow for the measurement of this new birefringence phenomenon, and for distinguishing it from similar birefringence phenomena which may be present. This "bi-axial Rosenfeld birefringence" is a scalar observable, and is supported in consequence both in achiral and chiral ensembles.

It is proportional to $E_0 B_0$ and vanishes only in achiral molecular point groups where all elements of the ORD polarisability vanish independently (see refs. [3] and [6] and the appendix). The discovery by FMD of this novel birefringence shows clearly the predictive abilities of computer simulation in non-linear optics, whose conventional theoretical methods have overlooked the existence of the phenomenon.

5. Discussion

FMD computer has been used to produce Kielich functions, and to demonstrate the existence of far infrared ORD (and by implication, CD). It has demonstrated the existence of bi-axial Rosenfeld birefringence in most achiral and all chiral ensembles.

The technique use in this first demonstration paper assumes that the ORD polarisability is frequency independent, and has also relied on a simple Lennard-Jones/partial charge model of the intermolecular potential energy. We have also been obliged to program an arbitrary sequence of numbers for the individual scalar elements of ${}^{m}\gamma^{e}_{ij}$ in (S)-CHBrClF due to a complete lack of ab initio or experimental information on ${}^{m}\gamma^{e}_{ij}$. From semi-classical perturbation theory [3] it is well known that the complete, complex, Rosenfeld tensor is frequency dependent, even in transparent regions of the spectrum far from optical resonance. In first order perturbation theory [6]

$$ {}^{m}\gamma^{e}_{ij} = \frac{2}{\hbar} \sum_{r \neq n} \rho_{nn} \frac{\omega(\omega^2_{rn} - \omega^2 - \Gamma^2_{rn})}{(\omega^2_{rn} - \omega^2 + \Gamma^2_{rn})^2 + 4\omega^2\Gamma^2_{rn}} \times \mathrm{Im}\langle n|m_i|r\rangle\langle r|\mu_j|n\rangle \,, \tag{36} $$

$$ {}^{m}\gamma'^{e}_{ij} = \frac{2}{\hbar} \sum_{r \neq n} \rho_{nn} \frac{\Gamma_{rn}(\omega^2_{rn} + \omega^2 + \Gamma^2_{rn})}{(\omega^2_{rn} - \omega^2 + \Gamma^2_{rn})^2 + 4\omega^2\Gamma^2_{rn}} \times \mathrm{Im}\langle n|m_i|r\rangle\langle r|\mu_j|n\rangle \,, \tag{37} $$

where $\langle r|\mu|n\rangle$ and $\langle r|m|n\rangle$ denote electric dipole and magnetic dipole transitions between the states $|n\rangle$ and $\langle r|$, respectively, with the frequency ω_{rn}; ρ_{nn} is the population of the system in the stationary state $|n\rangle$ and Γ^{-1}_{rn}, a characteristic relaxation time between states $|r\rangle$ and $|n\rangle$.

A precise description of the frequency dependence of the ORD polarisability ${}^{m}\gamma^{e}_{ij}$ clearly requires knowledge of what we are seeking, namely far infrared ORD and CD bandshapes over a range of frequencies from about 10 to 300 cm^{-1} [11–13]. It is equally clear that the FMD demonstration reported in this paper, and used to produce figs. 4–6, relies on approximating ${}^{m}\gamma^{e}_{ij}$ at one frequency, $\omega = \omega_1$, in eq. (36). In other words, we have coded in ${}^{m}\gamma^{e}_{ij}$ as nine different numbers, representing nine independent scalar elements of the C_1 symmetry molecular point group of (S)-CHBrClF.

Progress towards a better understanding of far infrared CD and ORD can be made by using a combination of experimental, theoretical and computational methods. Experimentally, CD and ORD is approaching [70] the far infrared range using Fourier transform interferometers. For example, Nafie et al. [70, 71] have provided data to about 300 cm^{-1} using a modified Nicolet

7199 interferometer with a piezo-optic modulator. By using a polarising wire grid beam divider, Polavarapu et al. [72] have demonstrated the feasibility of the far infrared CD and ORD interferometric technique to about $50\,cm^{-1}$.

Evans et al. [73–79] have made several inroads computationally towards an understanding of the fundamental rotation/translation molecular dynamics of chiral ensembles, using the enantiomers and racemic mixture of CHBrClF and other simple chiral structures small enough for computer simulation to be feasible with limited computer resource. This work was initiated in 1983 with the discovery of a well defined set of pseudo-scalar CCFs [73] in frame (1, 2, 3) of the principal molecular moments of inertia of CHBrClF that: (a) vanish in the laboratory frame (X, Y, Z) due to parity inversion symmetry, and (b) change sign between enantiomers in frame (1, 2, 3), vanishing in the racemic mixture. Although unobservable directly in frame (X, Y, Z) these "switching CCFs" characterise the fundamental, combined, molecular dynamics of rotation and translation and have been classified systematically [74] using group theoretical methods applied to ensemble thermodynamic averages, methods developed by Whiffen [75] and Evans [76]. Detailed and precise agreement has been obtained between computer simulation, including FMD, and group theoretical predictions in many molecular point groups [77], agreement on which CCFs vanish and which exist in both frames of reference. It has become clear that a complete understanding of the elements of molecular dynamics requires both frames of reference, and analytical theory must accordingly encompass this development.

FMD simulation of the interaction of electromagnetic plane waves with CHBrClF was initiated by Evans et al. [25] by considering a linear optical process, the torque between the permanent molecular electric dipole moment and the electric field of the plane wave. This method led to discernible differences in frame (1, 2, 3), but not in frame (X, Y, Z). For laboratory frame difference CFs the induction of electric and magnetic dipole moments is needed through the Rosenfeld polarisability tensors, as in the work, and this is a non-linear optical process. Recently, some semi-quantitative analysis has been made [78] linking far infrared ORD and CD to the possible observation of fundamental pseudoscalar CCFs such as that between the diffusing chiral molecule's center of mass linear velocity ($\boldsymbol{v}$) and its own angular velocity ($\boldsymbol{\omega}$). However, work for this paper has shown clearly, and for the first time, that a complete set of pseudoscalar difference CFs is generated directly in frame (X, Y, Z) through the intermediacy of appropriate components of the complex Rosenfeld tensor, the ORD (and CD) polarisabilities. One of these, the rotational velocity difference CF, is the direct Fourier transform of far infrared ORD, a pseudoscalar observable. Using the fundamental equations of motion of classical physics we have arrived at an understanding of Fresnel's discovery of 1824 [1] in terms of the motion and interaction of rigid, structurally chiral, molecules.

Bi-axial Rosenfeld birefringence of the type suggested by fig. 7 exists in principle not only in the far infrared range, but also in the infrared, visible, and ultraviolet, where it should be easily measurable by refractometry. It is characterised by a different refractive index in the propagation and orthogonal axes of a circularly polarised electromagnetic probe, a birefringence which should be identical for left and right components of the probe, but which should vanish when the probe is linearly or incoherently polarised. Its measurement gives unique information on off-diagonal elements in achiral molecular point groups of the Rosenfeld ORD polarisability. The only other contemporary sources of such information appear to be far more difficult to utilise because they are much smaller effects, for example magnetochiral birefringence [6, 80–86] (hitherto unmeasured) or light scattering in the presence of an electric field [87–89]. The only experimental difficulty in the measurement of Rosenfeld bi-axial birefringence appears to be in distinguishing it from any other birefringence effects which may be present. In principle, the method can be developed into a new spectral technique of considerable potential utility.

Acknowledgements

MWE and SW thank the Swiss NSF and the Canton and University of Zurich for funding this project. ETH Zurich is thanked for a major grant of IBM 3090 time to MWE, and Dr L.J. Evans for invaluable help with plotting the results on the University of Zurich, Irchel, mainframe laser plotter.

Appendix

Circularly polarised light induced energy of a molecule through the Rosenfeld tensor ${}^{m}\gamma^{e}$ (Langevin–Kielich functions)

In this paper we consider circularly polarised light propagating along the Z-axis of the laboratory frame $\{X, Y, Z\}$ and we also introduce the frame $\{1, 2, 3\}$ fixed in a molecule. If we denote the angle between the axis Z and the axis 1 by θ, we have the following transformation matrix elements between both frames described by Eulerian angles θ, ϕ and χ ($0 \leq \theta \leq \pi$, $0 \leq \phi \leq 2\pi$, $0 \leq \chi \leq 2\pi$):

$$\begin{aligned} e_{1X} &= \sin\chi \sin\theta , \\ e_{1Y} &= -\cos\chi \sin\theta , \\ e_{1Z} &= \cos\theta ; \end{aligned} \tag{A.1}$$

$$\begin{aligned} e_{2X} &= \cos\phi \cos\chi - \sin\phi \sin\chi \cos\theta , \\ e_{2Y} &= \cos\phi \sin\chi + \sin\phi \cos\chi \cos\theta , \\ e_{2Z} &= \sin\phi \sin\theta ; \end{aligned} \tag{A.2}$$

$$\begin{aligned} e_{3X} &= -\sin\phi \cos\chi - \cos\phi \sin\chi \cos\theta , \\ e_{3Y} &= -\sin\phi \sin\chi + \cos\phi \cos\chi \cos\theta , \\ e_{3Z} &= \cos\phi \sin\theta . \end{aligned} \tag{A.3}$$

The Langevin–Kielich functions, calculated analytically in this paper (eqs. (29) and (30)) and from molecular simulation, are defined as follows:

$$\langle e_{1Z}^2 \rangle = \langle \cos^2\theta \rangle = \frac{\int_0^{\pi} \cos^2\theta \sin\theta \int_0^{2\pi}\int_0^{2\pi} \exp[-E_n(\theta,\phi,\chi)/kT]\, d\chi\, d\phi\, d\theta}{\int_0^{\pi} \sin\theta \int_0^{2\pi}\int_0^{2\pi} \exp[-E_n(\theta,\phi,\chi)/kT]\, d\chi\, d\phi\, d\theta} \tag{A.4}$$

$$\langle e_{2Z}^2 \rangle = \langle \sin^2\phi \sin^2\theta \rangle = \frac{\int_0^{\pi} \sin^3\theta \int_0^{2\pi} \sin^2\phi \int_0^{2\pi} \exp[-E_n(\theta,\phi,\chi)/kT]\, d\chi\, d\phi\, d\theta}{\int_0^{\pi} \sin\theta \int_0^{2\pi}\int_0^{2\pi} \exp[-E_n(\theta,\phi,\chi)/kT]\, d\chi\, d\phi\, d\theta} \tag{A.5}$$

$$\langle e_{3Z}^2 \rangle = \langle \cos^2\phi \sin^2\theta \rangle = \frac{\int_0^{\pi} \sin^3\theta \int_0^{2\pi} \cos^2\phi \int_0^{2\pi} \exp[-E_n(\theta,\phi,\chi)/kT]\, d\chi\, d\phi\, d\theta}{\int_0^{\pi} \sin\theta \int_0^{2\pi}\int_0^{2\pi} \exp[-E_n(\theta,\phi,\chi)/kT]\, d\chi\, d\phi\, d\theta} \tag{A.6}$$

where $E_n(\theta, \phi, \chi)$ (eq. (4)) is the change in the potential energy of the molecule induced (in our case) by circularly polarised light and mediated by the Rosenfeld tensor:

$$E_n = -\tfrac{1}{2}{}^{e}\alpha_{ij}^{m}(-\omega, \omega) E_i^* B_j - \tfrac{1}{2}{}^{m}\alpha_{ij}^{e}(-\omega, \omega) B_i^* E_j + \text{c.c.} \tag{A.7}$$

Using the relations (1) and (11) we can write (A.7) in the form

$$E_n = \frac{i}{c} ({}^{m}\gamma_{XX}^{e} + {}^{m}\gamma_{YY}^{e})(\boldsymbol{E} \times \boldsymbol{E}^*)_Z , \tag{A.8}$$

where $(\boldsymbol{E} \times \boldsymbol{E}^*)_z$ is the Zth component of the product $\boldsymbol{E} \times \boldsymbol{E}^*$. To obtain eq. (A.8) we have taken into consideration the fundamental relations between the electric and magnetic field of the electromagnetic wave ($B_X = -(1/c)E_Y$,

$B_Y = (1/c)E_X$) which leads to

$$E_X^* B_X - E_X B_X^* = E_Y^* B_Y - E_Y B_Y^*$$
$$= \frac{1}{c}(E_X E_Y^* - E_Y F_X^*) = \frac{1}{c}(E \times E^*)_Z , \qquad (A.9)$$

$$E_X^* B_Y - E_X B_Y^* = E_Y^* B_X - E_Y B_X^* = 0 . \qquad (A.10)$$

The product $\boldsymbol{E} \times \boldsymbol{E}^*$ is pure imaginary for circularly polarised light [85] and for left (L) and right (R) cp waves (6)

$$(\boldsymbol{E} \times \boldsymbol{E}^*)_Z^{\mathrm{L}} = -(\boldsymbol{E} \times \boldsymbol{E}^*)_Z^{\mathrm{R}} = -\mathrm{i}E_0^2 . \qquad (A.11)$$

After transformation of the polarisability tensors ${}^m\gamma^e_{XX}$ and ${}^m\gamma^e_{YY}$ to the molecular frame, we have for the case (A.11)

$$E_n = \mp \frac{1}{c}(e_{X\alpha}e_{X\beta} + e_{Y\alpha}e_{Y\beta}){}^m\gamma^e_{\alpha\beta}E_0^2 , \qquad (A.12)$$

where the signs "−" and "+" stands for right and left cp light, respectively.

In general, for the lowest molecular symmetry (C_1), the tensor has 9 independent elements (see table A.1) and the energy (A.12) has the explicit form

$$E_n = \mp \frac{1}{c}\{2{}^m\gamma^e + \tfrac{1}{2}({}^m\gamma^e_{22} - {}^m\gamma^e_{33})$$
$$\times (e_{X2}^2 + e_{Y2}^2 - e_{X3}^2 - e_{Y3}^2)$$
$$- \tfrac{1}{3}[{}^m\gamma^e_{11} - \tfrac{1}{2}({}^m\gamma^e_{22} + {}^m\gamma^e_{33})](3e_1^2 - 1)$$
$$+ ({}^m\gamma^e_{12} + {}^m\gamma^e_{21})(e_{X1}e_{X2} + e_{Y1}e_{Y2})$$
$$+ ({}^m\gamma^e_{23} + {}^m\gamma^e_{32})(e_{X2}e_{X3} + e_{Y2}e_{Y3})$$
$$+ ({}^m\gamma^e_{13} + {}^m\gamma^e_{31})(e_{X3}e_{X1} + e_{Y3}e_{Y1})\}E_0^2 , \qquad (A.13)$$

where ${}^m\gamma^e = \frac{1}{3}{}^m\gamma^e_{\alpha\alpha} = \frac{1}{3}({}^m\gamma^e_{11} + {}^m\gamma^e_{22} + {}^m\gamma^e_{33})$ is the mean value of the tensor ${}^m\gamma^e$ and ${}^m\gamma^e_{11}$, ${}^m\gamma^e_{22}$, . . . denote the elements of ${}^m\gamma^e$ given in the molecular frame {1, 2, 3}.

If we use the relations (A.1)–(A.3) we obtain the energy (A.13) described by Eulerian angles,

$$E_n = \mp \frac{1}{c}\{2{}^m\gamma^e + \tfrac{1}{2}({}^m\gamma^e_{22} - {}^m\gamma^e_{33})\sin^2\theta\cos 2\phi$$
$$- \tfrac{1}{3}[{}^m\gamma^e_{11} - \tfrac{1}{2}({}^m\gamma^e_{22} + {}^m\gamma^e_{33})](3\cos^2\theta - 1)$$
$$- ({}^m\gamma^e_{12} + {}^m\gamma^e_{21})\sin\theta\sin\phi\cos\theta$$
$$- ({}^m\gamma^e_{13} + {}^m\gamma^e_{31})\cos\phi\sin\theta\cos\theta$$
$$- ({}^m\gamma^e_{23} + {}^m\gamma^e_{32})\sin\phi\cos\phi\sin^2\theta\}E_0^2 . \qquad (A.14)$$

The above energy does not depend on the angle χ. Substituting (A.14) into (A.4)–(A.6) we have the analytical expressions (29) for Langevin–Kielich functions, which were computed and compared with those from molecular simulation (figs. 2 and 3).

For molecules of water only ${}^m\gamma^e_{23}$ and ${}^m\gamma^e_{32}$ are

Table A.1
The rank 2 axial tensors ${}^m\gamma^e_{\alpha\beta}$ and ${}^m\gamma'^e$ for all point groups. The components of the polarisability tensors ${}^m\gamma^e_{\alpha\beta}$ and ${}^m\gamma'^e_{\alpha\beta}$ are denoted by the subscripts $\alpha\beta$ each of which, in the molecular system of coordinates, can take the value 1, 2, 3 (for the other point groups the components vanish).

Point group of the molecules	${}^m\gamma^e_{\alpha\beta}$ or ${}^m\gamma'^e_{\alpha\beta}$
C_1	11, 22, 33, 12, 21, 13, 31, 23, 32
C_2	11, 22, 33, 23, 32
C_{1h}	12, 21, 13, 31
D_2, C_{2v}	23, 32
C_3, C_4, C_6, C_∞	11, 22 = 33, 23 = −32
S_4	22 = −33, 23 = 32
D_3, D_4, D_6	11, 22 = 33
C_{3v}, C_{4v}, C_{6v}, $C_{\infty v}$	23 = − 32
D_{2d}	22 = −33
T, O, Y, K	11 = 22 = 33

non-zero and the energy (A.14) has the form

$$E_n = \pm \frac{1}{c}({}^m\gamma^e_{23} + {}^m\gamma^e_{32}) \sin\phi \cos\phi \sin^2\theta E_0^2 , \tag{A.15}$$

which leads to Langevin–Kielich functions (30). In eq. (A.15) the upper sign (+) is related to right and the lower sign (−) to left circularly polarised light.

References

[1] A. Fresnel, Bull. Soc Philomat. (1824) 147.
[2] S.F. Mason, BioSystems 20 (1987) 27.
[3] L.D. Barron, Molecular Light Scattering and Optical Activity (Cambridge University Press, Cambridge, 1982).
[4] L. Rosenfeld, Z. Phys. 52 (1928) 161.
[5] A. Moscowitz, Adv. Chem. Phys. 4 (1962) 67.
[6] S. Woźniak and R. Zawodny, Acta Phys. Pol. A 61 (1982) 175; 68 (1985) 675.
[7] S.F. Mason, Molecular Optical Activity and the Chiral Discriminations (Cambridge University Press, Cambridge, 1982).
[8] Ref. [3], ch. 7.
[9] L.A. Nafie and P.L. Polavarapu, J. Chem. Phys. 75 (1981) 2935, 2945.
[10] F. Cardelli and P Salvadori, eds., Optical Rotatory Dispersion and Circular Dichroism (Heyden and Son, London, 1973).
[11] M.W. Evans, G.J. Evans, W.T. Coffey and P. Grigolini, Molecular Dynamics (Wiley Interscience, New York, 1982).
[12] C. Brot, in: M. Davies, Senior Reporter, Dielectric and Related Molecular Processes, Vol. 2 (Chem. Soc., London 1975) p. 1 ff.
[13] G. Chantry, Submillimetre Spectroscopy (Academic Press, New York, 1971).
[14] M.W. Evans, J. Chem. Phys. 76 (1982) 5473, 5490; 77 (1982) 4632; 78 (1983) 925; 79 (1983) 5403.
[15] M.W. Evans, P. Grigolini and F. Marchesoni, Chem. Phys. Lett. 95 (1983) 548.
[16] M.W. Evans, P. Grigolini and F. Marchesoni, Chem. Phys. Lett. 95 (1983) 544.
[17] M.W. Evans, Phys. Lett. A 103 (1984) 323.
[18] M.W. Evans, Phys. Rev. A 30 (1984) 2062.
[19] M.W. Evans, G.C. Lie and E. Clementi, Chem. Phys. Lett. 138 (1987) 149.
[20] M.W. Evans, G.C. Lie and E. Clementi, J. Chem. Phys. 87 (1987) 6040.
[21] M.W. Evans, G.C. Lie and E. Clementi, Phys. Rev. A 36 (1987) 226.
[22] M.W. Evans, G.C. Lie and E. Clementi, J. Mol. Liq. 39 (1988) 39.
[23] M.W. Evans, G.C. Lie and E. Clementi, J. Mol. Liq. 40 (1989) 251.
[24] M.W. Evans, J. Phys. Chem. 92 (1988) 1639.
[25] M.W. Evans, G.C. Lie and E. Clementi, Z. Phys. D 7 (1988) 397.
[26] M.W. Evans, G.C. Lie and E. Clementi, Phys. Rev. A 37 (1988) 2551.
[27] M.W. Evans and D.M. Heyes, Comp. Phys. Rep. (Thematic Issue) 62 (1991) 249.
[28] M.W. Evans and D.M. Heyes, J. Phys. Chem. 95 (1991) 5287.
[29] S. Kielich, in ref. [12], Vol. 1 (1972).
[30] S. Kielich, Acta Phys. Pol. 36 (1969); A 37 (1970) 447, 719; J. Optoclectron, 2 (1970) 5.
[31] S. Kielich, Nonlinear Molecular Optics (Nauka, Moscow, 1982).
[32] Y.R. Shen, The Principles of Non-Linear Optics (Wiley, New York, 1984).
[33] C. Kalpouzos, D. McMorrow, W.T. Lottshaw and G.A. Kenney-Wallace, Chem. Phys. Lett. 150 (1988) 138.
[34] S. Feneuille, Rep. Prog. Phys. 40 (1977) 1257.
[35] W.A. Molander, C.R. Stroud, Jr. and J.A. Yeazell, J. Phys. 19 (1986) L461.
[36] S. Kielich, Acta Phys. Polon. 36 (1969) 621.
[37] K. Knast and S. Kielich, Acta Phys. Polon. 55A (1979) 319.
[38] S. Kielich, Opt. Commun. 1 (1969) 129.
[39] S. Kielich and R. Zawodny, Physica B 89 (1977) 122.
[40] M.W. Evans and G. Wagniere, Phys. Rev. A 42 (1990) 6732.
[41] M.W. Evans, S. Woźniak and G. Wagnière, Physica B 173 (1991) 357.
[42] M.W. Evans and S. Woźniak, Physica B 179 (1992) 6.
[43] M.W. Evans, S. Woźniak and G. Wagnière, Physica B 175 (1991) 412.
[44] M.W. Evans, S. Woźniak and G. Wagnière, Physica B 176 (1992) 33.
[45] S. Kielich, N.L. Manakov and V.D. Ovsianikov, Acta Phys. Polon. 53A (1978) 581, 595, 737.
[46] M.W. Evans, J. Phys. Chem. 95 (1991) 2256.
[47] M.W. Evans, Chem. Phys. 157 (1991) 1.
[48] P.S. Pershan, Phys. Rev. 130 (1963) 919.
[49] J.P. van der Ziel, P.S. Pershan and L.D. Malmstron, Phys. Rev. Lett. 15 (1965) 190.
[50] J.P. van der Ziel, P.S. Pershan and L.D. Malmstron, Phys. Rev., 143 (1966) 574.
[51] M.W. Evans, I. Prigogine and S.A. Rice, eds., Advances in Chemical Physics, Vol. 63 (Wiley Interscience, New York, 1985).
[52] M.W. Evans, W.T. Coffey and P. Grigolini, Molecular Diffusion (Wiley Interscience, New York, 1984; MIR, Moscow, 1988) Ch. 1 and 2.
[53] M.W. Evans, G.J. Evans and A.R. Davies, in: I. Prigogine and S.A. Rice, eds., Advances in Chemical Physics (Wiley Interscience, New York, 1980) vol. 44.

[54] M.W. Evans, P. Grigolini, G. Pastori-Parravicini, I. Prigogine and S.A. Rice, eds., Advances in Chemical Physics, Vol. 62 (Wiley Interscience, New York, 1985).
[55] J.S. Rowlinson and M.W. Evans, Annu. Rep. Prog. Chem. 72A (1975) 5.
[56] R.R. Birss, Symmetry and Magnetism, 2nd Ed. (North-Holland, Amsterdam, 1966).
[57] S. Kielich, Prog. Opt. 20 (1983) 155.
[58] M.W. Evans, J. Chem. Soc., Faraday Trans. 2 70 (1974) 1620.
[59] L.D. Barron, Chem. Soc. Rev. 15 (1986) 189.
[60] M.W. Evans, Phys. Lett. A 146 (1990) 185, 475.
[61] M.W. Evans, Chem. Phys. Lett. 152 (1988) 33.
[62] M.W. Evans, in: I. Prigogine and S. A. Rice, eds., Advances in Chemical Physics, Vol. 81 (Wiley Interscience, New York, 1992) p. 361 (a review with approx. 450 references, in press, code TETRA listed in full).
[63] M.W. Evans, W. Luken, S. Chin, M. Re and G. Gurst, IBM Kingston Group Videos, Clementi Organisation, Dept. 48B/428, IBM, Kingston, New York, 1986–1988, animations of water, benzene, hexafluorobenzene, carbon tetrachloride, methyl hexa-tri-yne, CHBrClF, and field effects, code TETRA.
[64] M.W. Evans and C.R. Pelkie, IBM Supercomputer Competition and Proceedings (1991) in press; J. Opt. Soc. Am. B, in press. (half hour animation in colour of optical Zeeman effects in (S)-CHBrClF; code TETRA. Narration by C.R. Pelkie, to be distributed by Media Magic, California © M.W. Evans, Cornell Theory Center, Visualization Unit, 1989/1990).
[65] M.W. Evans, J. Chem. Soc., Chem. Commun. (1983) 139.
[66] D. Fincham and D.M. Heyes, in ref. [51].
[67] M.W. Evans, J. Mol. Liq. 32 (1986) 173.
[68] M.W. Evans, K.N. Swamy, K. Refson, G.C. Lie and E. Clementi, Phys. Rev. A 36 (1987) 3935.
[69] M.W. Evans, G.C. Lie and E. Clementi, J. Chem. Phys. 88 (1988) 5157.
[70] S.J. Giancorsi, K.M. Spencer, T.B. Freedman and L.A. Nafie, J. Am. Chem. Soc. 111 (1989) 1913.
[71] T.B. Freedman, M. Germana-Paterlini, Nam Soo Lee and L.A. Nafie, J. Am. Chem. Soc. 109 (1987) 4727.
[72] P.L. Polavarapu, P.G. Quincey and J.R. Birch, Infrared Phys. 30 (1990) 175.
[73] M.W. Evans, Phys. Rev. Lett. 50 (1983) 371.
J. Chem. Soc., Faraday Trans 2 79 (1983) 1331, 1811.
M.W. Evans, J. Baran and G.J. Evans, J. Chem. Soc., Faraday Trans. 2 79 (1983) 1473.
[74] M.W. Evans, Phys. Rev. A 39 (1989) 6041.
[75] D.H. Whiffen, Mol. Phys. 63 (1988) 1053.
[76] M.W. Evans, Chem. Phys. 128 (1988) 413; 132 (1989) 1; 135 (1989) 187; Mol. Phys. 71 (1990) 193.
[77] M.W. Evans and D.M. Heyes, Phys. Scripta 42 (1990) 96.
[78] M.W. Evans, J. Mol. Liq. 47 (1990) 109.
[79] M.W. Evans and G.J. Evans, Phys. Rev. Lett. 55 (1985) 818.
[80] S. Woźniak and R. Zawodny, Phys. Lett. A 85 (1981) 111.
[81] G. Wagnière and A. Meier, Chem. Phys. Lett. 93 (1982) 78.
[82] G. Wagnière and A. Meier, Experientia 39 (1983) 1090.
[83] G. Wagnière, Z. Naturforsch. A 39 (1984) 254.
[84] L.D. Barron and J. Vrbancich, Mol. Phys. 51 (1984) 715.
[85] G. Wagnière, Phys. Rev. A 40 (1989) 2437.
[86] M.W. Evans, Physica B 168 (1991) 9.
[87] A.D. Buckingham and R.A. Shatwell, Phys. Rev. Lett. 45 (1980) 21.
[88] S. Woźniak, Phys. Lett. A 148 (1990) 188.
[89] S. Woźniak and S. Kielich, J. Chem. Phys. 94 (1991) 7588.